

ISVR Technical Report

SCIENTIFIC PUBLICATIONS BY THE ISVR

Technical Reports are published to promote timely dissemination of research results by ISVR personnel. This medium permits more detailed presentation than is usually acceptable for scientific journals. Responsibility for both the content and any opinions expressed rests entirely with the author(s).

Technical Memoranda are produced to enable the early or preliminary release of information by ISVR personnel where such release is deemed to be appropriate. Information contained in these memoranda may be incomplete, or form part of a continuing programme; this should be borne in mind when using or quoting from these documents.

Contract Reports are produced to record the results of scientific work carried out for sponsors, under contract. The ISVR treats these reports as confidential to sponsors and does not make them available for general circulation. Individual sponsors may, however, authorize subsequent release of the material.

COPYRIGHT NOTICE

(c) ISVR University of Southampton All rights reserved.

ISVR authorises you to view and download the Materials at this Web site ("Site") only for your personal, non-commercial use. This authorization is not a transfer of title in the Materials and copies of the Materials and is subject to the following restrictions: 1) you must retain, on all copies of the Materials downloaded, all copyright and other proprietary notices contained in the Materials; 2) you may not modify the Materials in any way or reproduce or publicly display, perform, or distribute or otherwise use them for any public or commercial purpose; and 3) you must not transfer the Materials to any other person unless you give them notice of, and they agree to accept, the obligations arising under these terms and conditions of use. You agree to abide by all additional restrictions displayed on the Site as it may be updated from time to time. This Site, including all Materials, is protected by worldwide copyright laws and treaty provisions. You agree to comply with all copyright laws worldwide in your use of this Site and to prevent any unauthorised copying of the Materials.

UNIVERSITY OF SOUTHAMPTON
INSTITUTE OF SOUND AND VIBRATION RESEARCH
FLUID DYNAMICS AND ACOUSTICS GROUP

**Commentary on the detection of bubble activity generated in ex-vivo tissue by
High Intensity Focused Ultrasound (HIFU) with respect to the generation of
therapeutic lesions in tissue for the treatment of cancer**

by

J. McLaughlan, I. Rivens, T. G. Leighton and G. ter Haar

ISVR Technical Report No. 330

April 2010

Authorized for issue by
Professor R J Astley, Group Chairman

© Institute of Sound & Vibration Research

ACKNOWLEDGEMENTS

This work was supported by the EPSRC, grant number GR/SR64042. The experiments were conducted at the Institute of Cancer Research, Joint Department of Physics, Royal Marsden NHS trust, Sutton, Surrey, SM2 5PT, UK (the host institution of authors JM, IR and GtH). The authors would like to thank Dr. Constantin Coussios of Oxford University for extremely helpful advice and discussions relating to this project. The authors are grateful to Dr Peter Birkin of the University of Southampton School of Chemistry for assistance with the sonochemical tests.

CONTENTS

ACKNOWLEDGEMENTS	II
FIGURE CAPTIONS	V
ABSTRACT	IX
ABSTRACT	IX
1 INTRODUCTION	10
2 METHODS	11
2.1 Data acquisition	11
2.2 Data processing	14
2.3 Tissue studies	16
2.4 Degassed water studies	19
2.5 Sonochemical studies	19
3 RESULTS	21
3.1 Measurements in degassed water	21
3.2 Sonochemical study	30
3.3 Ex-vivo tissue experiments	35
4 THEORY	37
4.1 Scattering cross-section	37
4.2 Radiated pressure from a resonant bubble	40
5 DISCUSSION	43
5.1 Degassed water studies	43

5.2	Sonochemical study	47
6	CONCLUSIONS	48
7	REFERENCES	49

FIGURE CAPTIONS

- Figure 1.** A side (left) and plan views (right) of the experimental set-up used for the degassed water and ex-vivo tissue study. The tank is omitted from the plan view, for clarity..... 11
- Figure 2.** A photograph of the pulse echo target mounted on the 10 MHz passive transducer. The 2 mm ball is located at the transducers focus..... 13
- Figure 3.** A high broadband frequency spectrum (4.0-12.5 MHz) recorded at 1 s (using 2^{13} data points) 1s into the 4 s HIFU exposure at an I_{sp} of 2200 W/cm^2 , (-2.32 MPa) of degassed water without software filtering (a) and with software filtering (b). This was the highest exposure used for this study. 15
- Figure 4.** The averaged peak amplitude of the detected half harmonic emissions, separated into exposures performed on 1 and 2 day old tissue. Uncertainty shown in the data is the standard deviation, where the number of exposures ($n = 4-6$)..... 17
- Figure 5.** Cylindrical Perspex tissue holder used in both degassed water and ex-vivo experiments. The Front face is shown in (a) and the side view (b) shows length of the holder with the front face to the left hand side and the back face to the right hand side. A diagnostic imaging probe was located above the cylinder at approximately the position of the double headed arrow in (b). For clarity, Mylar windows are not shown in either frame. 18
- Figure 6.** Photographs of the front (a) and side (b) of the cylindrical Perspex holder, which contained the KI solution used for the sonochemical study. The two pieces of cling film used to provide the front sides and rear acoustic windows are not shown in the photograph. The frosted part of the holder shown in (b) was slotted into the Perspex block which held the rear acoustic window in place and located the sample holder in the acoustic field..... 20
- Figure 7.** The low (a-c) and high (d-f) frequency spectra detected at three separate times (0.3, 0.9 and 1.4 s) during a 4 s HIFU exposure, [$I_{sp} = 1100 \text{ W/cm}^2$ (2.10 MPa)] of degassed water. A Hanning window function and 2^{13} data points were used to generate each of the FFT spectra. The red dashed line indicates the peak noise level measured during a sham exposure..... 22

- Figure 8.** Sample spectra acquired from three individual 4 s HIFU exposures in degassed water, with I_{sp} (pressure) of (a-c) 300 W/cm² (1.43 MPa), (d-f) 1100 W/cm² (2.10 MPa) and (g-i) 2200 W/cm² (2.32 MPa). (a, d and g) Half harmonic (0.846 MHz) emissions, (b, e and h) fourth harmonic and (c, f and i) integrated (4-12 MHz) broadband emissions. The red dashed line indicates the peak noise level measured during a sham exposure. 23
- Figure 9.** The electrical drive power derived from the measured HIFU drive voltage and current is shown for the three exposures in degassed water shown in Figure 8. (a) 300 W/cm² (1.43 MPa), (b) 1100 W/cm² (2.10 MPa) and (c) 2200 W/cm² (2.32 MPa). The power scale has been expanded to show the range of fluctuation, approximately $\pm 3\%$ about the nominal drive level..... 23
- Figure 10.** Cavitation monitoring measurements made between 2.38 and 2.40 s into 4 s long 1100 W/cm² (2.10 MPa) (a-d) and 2200 W/cm² (2.34 MPa) (e-h) exposures in degassed water. (a, e) Drive power, (b, f) fourth harmonic, (c, g) broadband emissions and (d, h) half harmonic. The red dashed line indicates the peak noise level measured from a sham exposure. 24
- Figure 11.** The spectral content of the drive voltage at 2.39 s for (a) 1100 W/cm² and (b) 2200 W/cm² exposures in degassed water. This shows that the fluctuations are dominated by the fundamental frequency (1.69 MHz). 25
- Figure 12.** Two ultrasound imaging frames (72 ms resolution) taken during a single 4 s 1700 W/cm² (2.30 MPa) exposure in degassed water 0.21 (a) and 2.43 s (c) into the exposure. Panels (b) and (d) are frequency maps, with a linear colour scale (V_{rms}), from (a) and (b), respectively. The HIFU focal plane is at 0 mm (in b and d) with the beam incident from the right (in all figures except e). (e) shows the corresponding audible emissions (50 ms resolution), on a power colour scale (dB). The maximum emissions lie between 16-18 kHz..... 26
- Figure 13.** Drive power and acoustic emission data (1 ms resolution) from the exposure shown in Figure 12. The fourth harmonic data has been omitted as it showed a similar trend to the broadband emissions. The time scale was chosen to show emissions at the same times (left column at 0.21 and right column at 2.43 s) as shown in Figure 10, within the temporal resolution of the microphone system (± 0.05 s). 27
- Figure 14.** The percentage of exposures in which acoustic spectra with amplitudes exceeding the noise level a minimum of 5 times during the 4 s exposures were

detected. The signals were measured over the range 300-2200 W/cm ² (1.48-2.32 MPa) where $n = 3-5$ for each exposure level.	28
Figure 15. The averaged total time integrated (a) ultraharmonic (7.62 MHz), (b) HF broadband emissions (4-12 MHz), (c) LF broadband emissions (0.1-0.8 MHz), (d) half harmonic (0.846 MHz) and (e) fourth harmonic (6.77 MHz) shown over the range of peak negative pressures used. Uncertainty, where shown, is the standard deviation for $n = 3-5$. The red dashed line indicates the peak noise level measured from sham exposures.	29
Figure 16. Acoustic spectra detected with the passive cavitation detection system from a single 10 s exposure at 1700 W/cm ² (2.30 MPa) in the KI solution. The red dashed line indicates the peak noise level measured from a sham exposure..	31
Figure 17. Acoustic spectra detected with the passive cavitation detection system from a single 10 s exposure at 3100 W/cm ² (2.38 MPa) in the KI solution. The red dashed line indicates the peak noise level measured from a sham exposure..	32
Figure 18. The measured absorbance over the UV spectra of the two KI solutions from the exposures described in (a) Figure 16 and (b) Figure 17 . The uncertainty shown in the plots is the measured variation in absorbance at 350 nm of an unexposed sample.	32
Figure 19. The averaged total time integrated (a) ultraharmonic (7.62 MHz), (b) HF broadband emissions (6-10 MHz), (c) LF broadband emissions (0.1-0.8 MHz), (d) half harmonic (0.846 MHz) and (e) fourth harmonic (6.77 MHz) shown over the range of peak negative pressures used. Uncertainty, where shown, is the standard deviation for $n = 3-5$. The red dashed line indicates the peak noise level measured from sham exposures.	33
Figure 20. The measured absorbance (ABS) of UV at 350 nm in KI solutions exposed for 5, 10 and 16 s. The uncertainty shown is that of the measured absorbance at 350 nm of an unexposed sample.	34
Figure 21. The audible emissions detected (in air) when ex-vivo porcine muscle was heated using microwave energy, shown on a power colour scale (dB) – note that the scale used is different to that for measurements made in water (e.g. Figure 12) and indeed conversion between the two media is not simple (Finfer et al., 2008). Emissions commence at $t = 0$ s when the tissue is removed from the microwave and placed next to the microphone. Signals prior to this time represent background noise in the laboratory.	35

Figure 22. Half harmonic (a), fourth harmonic (b) and broadband emissions (c) for a 120 s free-field exposure at I_{sp} 290 W/cm ² (1.32 MPa) in ex-vivo liver tissue. Note the scaling factor of 10 ⁻⁵ on (a) and (b). All values plotted on these graphs are either equal to or less than the peak noise level measured from a sham exposure (red dashed line). Diagnostic imaging was not used during this exposure.	36
Figure 23. The acoustic scattering cross-sections for a range of bubble sizes, 0.1-10 μm (a) and 0-3.0 mm (b) exposed to 1.69 MHz ultrasound.	38
Figure 24. The acoustic scattering cross-sections for a range of bubble sizes, 0.1-3 μm (a) and 0-3.0 mm (b) exposed to 6.77 MHz ultrasound (i.e. the 4 th harmonic of the HIFU drive signal).	39
Figure 25. (a) The measured amplitude spectrum (0.01-15 MHz) of individual harmonics, in an 80 cycle HIFU pulse at 47.5 W electrical drive power. (b) Percentage contribution to the time-domain signal of the first 8 harmonics. This was calculated from the total time-domain signal divided by the contribution of each harmonic.	40
Figure 26. The pressure radiated by a resonant bubble as a function of distance from the bubble wall, r . Four points during the collapse of the bubble are shown, which are $R = R_{max}$ (a), $R = 0.75 * R_{max}$ (b), $R = 0.50 * R_{max}$ and $R = 0.25 * R_{max}$ ($R_{max} = 2.6 \mu\text{m}$).	42
Figure 27. The calculated attenuation at four frequencies with increase depth in liver tissues, which correspond to the half harmonic (0.85 MHz), drive (1.70 MHz), fourth harmonic (6.77 MHz) and the centre frequency of the broadband emission range (8.00 MHz) monitored in this study.	45

ABSTRACT

Cancer treatment by extracorporeal high intensity focused ultrasound (HIFU) is constrained by the time needed to ablate relevant tumour volumes clinically. Controlled cavitation might be used to optimise HIFU treatments, but such control requires a greater understanding of its role in lesion formation, and the provision of appropriate techniques to monitor cavitation in tissue. During HIFU exposure various forms of cavitation can occur: acoustic cavitation (both non-inertial and inertial), and bubble formation due to two thermally-driven effects (the vaporisation of liquid into vapour, and the exsolution of formerly dissolved permanent gas out of the liquid and into gas spaces). Different forms of cavitation gives rise to characteristic signals that can be monitored during HIFU. Furthermore, the character of the signal can change depending on the stage of the cavitation in question (nucleation, established cavitation, population effects etc.). Prior to undertaking experiments using tissue, studies were performed by exposing degassed water. The aim of these experiments was to test a detection system in a minimally attenuating medium known to cavitate, in order to provide data for comparison with ex-vivo tissue results.

This report is written in support of the journal paper “A Study of Bubble Activity Generated in Ex-Vivo Tissue by High Intensity Focused Ultrasound (HIFU)” by the same authors (McLaughlan *et al.* 2010). It outlines supporting material for the discussion and conclusions contained in that paper, a study involving monitoring clinically relevant HIFU exposures in degassed water and ex-vivo bovine liver. Monitoring is accomplished using a suite of cavitation detection techniques (exploiting passive and active acoustics, audible and ultrasonic emissions and electrical drive power fluctuations). The aim of the paper is to allow informed progress towards a monitoring system specifically tailored for use during clinical HIFU treatments.

A web page containing sound files associated with this report is available at <http://www.isvr.soton.ac.uk/fdag/HIFU.HTM>

1 Introduction

A considerable obstacle to the more extensive use of extracorporeal high intensity focused ultrasound (HIFU) in the treatment of cancer is the time required to ablate clinically relevant tumour volumes. Although it is thought that cavitation could be used to optimise HIFU treatments, there remains ambiguity as to its role during lesion formation in tissue. Differentiation between acoustic cavitation (non-inertial and inertial) effects and those caused by cavitation due to thermal exsolution of previously-dissolved gas and gas vapour release ('boiling') is required as a prerequisite for an understanding of the processes involved. Although the term 'boiling' refers to the thermodynamically-driven process of transition from the liquid to gas phase which occurs when the vapor pressure of a specified liquid equals the ambient (usually atmospheric) pressure, in HIFU, the term 'boiling bubbles' is colloquially used to describe the macroscopic bubbles which grow in tissue as a result of the thermally induced processes of vaporization of the liquid and exsolution of previously-dissolved gas. As such, 'boiling' bubbles can form below the boiling point of the liquid components of the tissue in question. The aim of the present experiments was to test a detection system in a minimally attenuating medium known to cavitate (Flynn, 1964; Neppiras, 1980; Walton and Reynolds, 1984) in order to give data for comparison with ex-vivo tissue results. Since the acoustic absorption of water is negligible, focal heating is unlikely, and thus cannot affect acoustic cavitation, and "boiling" bubbles cannot be generated. However, in water, radiation force will result in streaming of both the fluid and the cavitation bubbles to a far greater extent than would occur in soft tissue, effects which, for example, change the distribution of nuclei and homogenise concentrations of dissolved gas (Leighton, 1995). This study tested our cavitation detection system in an initial investigation of bubble activity induced during clinically relevant HIFU exposures in degassed water, sonochemical solution and ex-vivo bovine liver. A sonochemical reaction was used as an indicator of inertial cavitation in order to aid interpretation of the emissions detected by a passive cavitation detection system. After using these studies to identify which cavitation measures were most useful for HIFU purposes, the next step would be to optimised system hardware and software for clinical use. This report provides supplementary evidence and discussion in support of McLaughlan *et al.* (2010).

2 Methods

2.1 Data acquisition

A 1.69 MHz focused bowl piezoceramic transducer (f-number 1.79, focal length 15 cm) was used, in the configuration shown in Figure 1, for these studies. Transducer output was calibrated separately for the total power (intensity) and the peak negative pressure using the following two techniques. HIFU intensity was determined using a horizontally aligned radiation force balance in degassed water (Hill *et al*, 1994). Free-field peak-negative pressure values were measured with a 0.5 mm element PVDF membrane hydrophone (GEC Marconi, UK) using 80 cycle pulses. The free-field intensity and pressure were corrected to give *in-situ* levels using an attenuation value of 0.11 Np/cm at 1.7 MHz for liver (Duck, 1990), neglecting the effects of non-linear propagation in the HIFU field. All HIFU exposures are quoted as *in-situ* spatial-peak intensities (I_{sp}) obtained using the calculation suggested by Hill *et al*, (1994) with the *in-situ* focal peak negative pressure, in MPa, indicated in brackets.

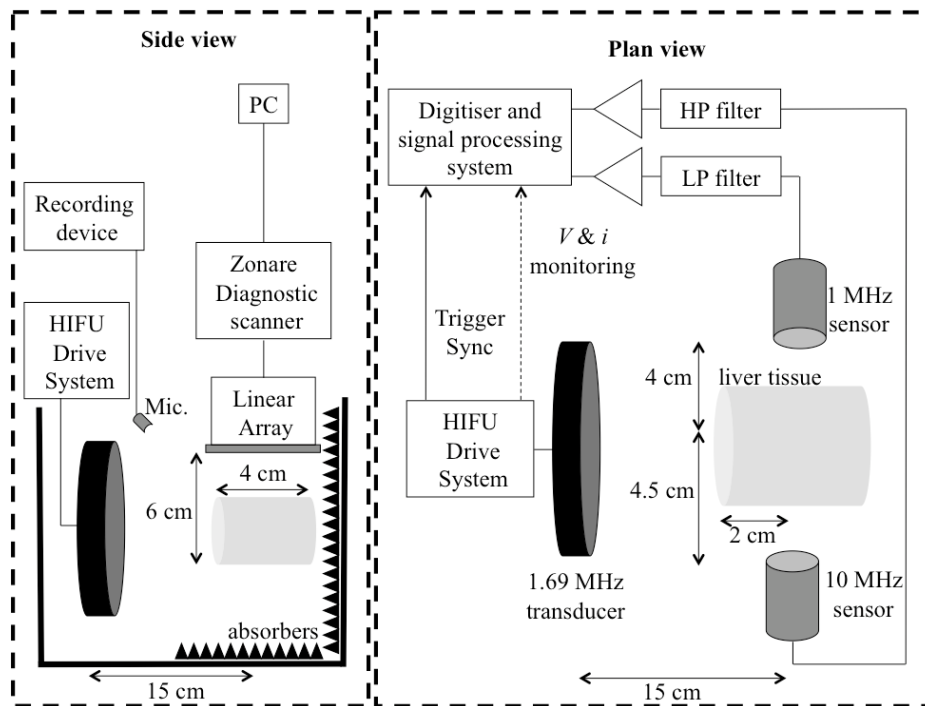


Figure 1. A side (left) and plan views (right) of the experimental set-up used for the degassed water and ex-vivo tissue study. The tank is omitted from the plan view, for clarity.

A timer, (0.01 s resolution) built in house, was used to control exposure duration by triggering both a function generator (Agilent, 33120A) and a data acquisition system (detailed below). The amplified (ENI A300 amplifier, +55 dB) signal was connected to the HIFU transducer through a voltage (V) and current (i) ‘pick-off’ box, allowing $V/1000$, $V/20$ and $i*10$ to be monitored simultaneously. A passive cavitation detection (PCD) system, consisting of the two focused transducers (Olympus NDT Inc, Waltham, MA, USA) detailed in Table 1 was used to allow simultaneous investigation of different acoustic emissions. Specifically, the half harmonic (0.845 MHz) was investigated using the low frequency detector (LF PCD), and the 4th superharmonic (6.77 MHz) and high frequency broadband emissions (4-12 MHz) were studied using the high frequency detector (HF PCD).

	Frequency (MHz)	Bandwidth (MHz)	Diameter (cm)	Focal length (cm)	Radial FWHM (mm)	Axial FWHM (mm)
LF PCD	1	0.1-2	1.5	4.0	2.0	30.0
HF PCD	10	5-12	3.0	4.5	4.0	15.0

Table 1. Technical specifications for the passive sensors that were used in this study.

For each PCD transducer a filter (Allen Avionics) was used - low pass (LP) (F5099, frequency cut off 850 kHz, 80 dB attenuation at 1.69 MHz, 25 dB/decade) and high pass (HP) (F5100, frequency cut off 6 MHz, 90 dB attenuation at 1.69 MHz, 25 dB/decade) to minimise the amount of drive signal picked up. A 20 dB preamplifier (Advance Receiver Research, 7866, 0.1-30 MHz bandwidth) was used with each detector to improve signal digitisation. Even though the system allowed monitoring of the 4th, 5th 6th and 7th superharmonics, the 4th harmonic was chosen since it was the first harmonic outside the high pass frequency band and would, after transit through an attenuating medium such as ex-vivo tissue, provide a greater signal strength than the higher harmonics. The data acquisition system (DAQ) used in this study had two 8-bit 4-channel boards (Spectrum Inc. MI.2031 and MI.2021 with sample rates of up to 200 MHz and 50 MHz, respectively) installed in a dual PCI bus PC (Supermicro, USA, Pentium 4, 4 GB RAM). The dual PCI bus allowed data from both cards to be streamed directly to computer RAM using a first in, first out (FIFO) function built into the cards. A C++ program was used to control the FIFO mode of the acquisition

cards and to record uninterrupted data for up to 5 s at rates up to 50 MHz (for both detectors) and 15 MHz (V and i). Although large amounts of data could be recorded over entire exposure periods (~ 125 MB/s), it was not possible to process the data to allow display of acoustic emissions in real time. These sample rates meant that the PCD system was unsuitable for signals >25 MHz.

The right hand schematic in Figure 1 shows a top down view of the PCD system used for the ex-vivo study. It shows the diagnostic scanner (Zonare Z.One), with an L10.5 probe (centre frequency 8 MHz, MFCD1313, 14 Hz frame rate, 6 cm imaging depth), which could be used before during and after HIFU exposure. This study did not use gating techniques, and so there was acoustic interference due to the HIFU signal during the acquisition of real-time B-mode images during HIFU exposure. Similarly, the diagnostic scanner created acoustic interference in the form of additional signals which were detected by the PCD transducers. Each image frame was downloaded to a PC after each acquisition, and the IQ data was converted to RF and B-mode data using a MatLab routine provided by Zonare.

The 1 MHz sensor was aligned with the focal peak of the HIFU, by reflecting a 40 cycle HIFU burst (~ 0.2 % duty cycle) from a target (Figure 2) that had initially been pulse-echo located at the HIFU focus. As this target was constructed to be in the focal zone of the 10 MHz sensor it was aligned by default. Finally, the diagnostic imaging array was aligned with the focal peak by placing it at the position in which the maximum reflection from the ball bearing was observed.

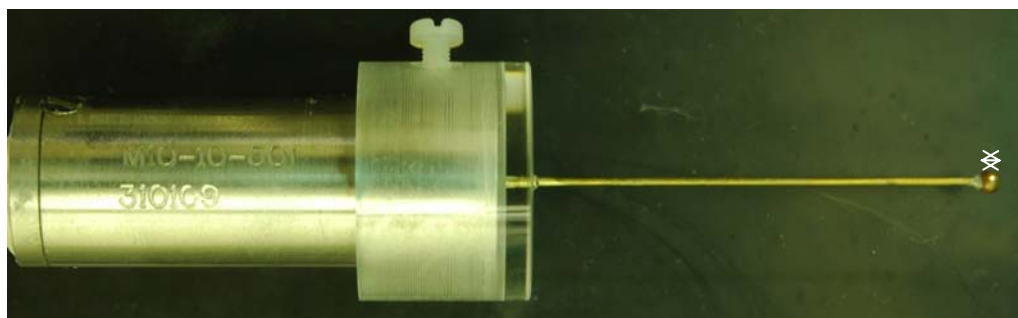


Figure 2. A photograph of the pulse echo target mounted on the 10 MHz passive transducer. The 2 mm ball is located at the transducers focus.

The passive cavitation detection sensor was connected directly into the DAQ. A microphone (Partridge Electronics, Essex, UK, CHK00627, frequency response 0.03-17 kHz, 80 dB signal/noise) connected to a digital recording device (shown in Figure 1) was used to encode audible emissions at a rate of 44 kHz with 16-bit resolution. The frequency information was analysed with a temporal resolution of 47 ms using a MatLab routine.

2.2 Data processing

The average electrical power (P) was calculated from the measured $V/1000$ and $i*10$ using:

$$P = \frac{1}{N\tau} \int_0^{N\tau} V(t)i(t)dt \quad (1)$$

where the integration was performed over N acoustic cycles (500) with period τ .

The (~1 GB) data set for each PCD transducer was sub-divided into groups of between 2^{12} - 2^{14} points (resulting in a temporal resolution of 1 ms and a spectral resolution of 1.5 kHz) and an FFT (fast Fourier Transform) calculation using a ‘Hanning’ window function was performed on each group. Instead of analysing the entire frequency spectrum variation over time, specific frequencies or frequency ranges of interest were identified. For the LF PCD the half-harmonic, 0.846 MHz was studied and the fourth, fifth and sixth harmonics plus broadband were investigated using the HF PCD. For each data set, the peak spectral amplitudes were recorded over the entire exposure time, and plotted as a function of time. Broadband emissions were obtained using a two step process. Firstly, a ‘comb’ software filter was used to remove any contribution from the harmonics produced by non-linear propagation and harmonics of the subharmonic (as shown in Figure 3). This software filter sets the amplitude of the spectrum for a region 0.2 MHz wide around each harmonic to zero, as shown in Figure 3(a). This process leaves only broadband frequency information, as shown in Figure 3(b). Secondly, integration over the discontinuous frequency band shown in Figure 3(b) gives the amplitude of broadband emissions. The process of removing harmonics from broadband data was repeated over each data set for both the

1 and 10 MHz cavitation detectors, making it possible to study both high and low frequency broadband emission variation during each exposure.

When it was not possible to obtain continuous data throughout an exposure (for exposures longer than 16 s), proprietary oscilloscope software (SBench) was used with the DAQ system to acquire data (at up to 50 MHz) at regular intervals during single 2-5 s HIFU exposures. This allowed real time inspection of the detected spectrum. However, the data could only be stored discontinuously. This acquisition mode meant that it was possible to acquire for much longer times (>16 s). Using this mode the acquisition software stored 2^{13} samples at a rate of 25 Hz, each acquisition providing a snap shot of the acoustic emissions.

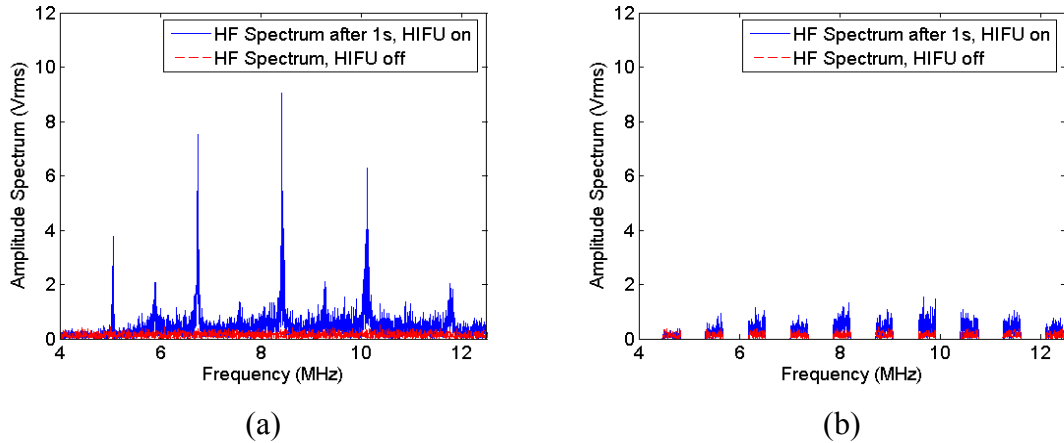


Figure 3. A high broadband frequency spectrum (4.0-12.5 MHz) recorded at 1 s (using 2^{13} data points) 1s into the 4 s HIFU exposure at an I_{sp} of 2200 W/cm^2 , (-2.32 MPa) of degassed water without software filtering (a) and with software filtering (b). This was the highest exposure used for this study.

In order to estimate the noise level in the system, a sham exposure was carried out each time a set of experiments were performed. This was done at the highest drive level used for the experiment with the HIFU transducer disconnected from the drive chain, but with the power amplifier switched on (open circuited). This measurement allowed estimation of the noise detected by the system for a single exposure, which could vary depending on the combination of sensors/filters/amplifiers used. In addition, the acquisition time was always longer than the HIFU exposure and the ‘off time’ data was used to provide a further estimate of the noise level in the system,

when the RF drive chain was not actively driven. For data processing purposes, the noise level was defined as twice the peak detected value, either from sham or ‘off time’ measurements (the larger of the two). For both the water and ex-vivo tissue studies the noise levels for this detection system were 14 μ Vrms for half, 20 μ Vrms for fourth harmonic detection and 10 mVrms.Hz for integrated broadband emissions. These levels are depicted in the figures presented in the results by dashed red lines. The MatLab routine that was used to decide whether a signal was above noise or not (in order to determine whether a particular signal was definitely detected during an exposure) contained more stringent conditions. Detected spectra were required to exceed twice the noise level for a minimum of five (none of which need be sequential) data points in order to avoid any noise artifacts lasting up to 5 ms being misinterpreted as a cavitation event. These more stringent conditions were used since the binary output of this program needed, for example, to be insensitive to, the noise spikes that were sometimes generated from switching on/off the HIFU drive system, in an attempt to reduce the chances of false positive identification of acoustic cavitation activity.

2.3 Tissue studies

Freshly excised ex-vivo bovine liver, collected from an abattoir and stored overnight in a refrigerated room (5-10°C), was cut into cylindrical samples (50 mm diameter and 45 mm long), submerged in degassed water, and degassed for either 1 h (on the first day after collection) or for 2 h (on the second day after collection). This different procedure is necessary because the older tissue will have undergone more autolysis, and thus has greater gas content. Water was degassed by holding unfiltered tap water under a vacuum of 0.85 MPa for at least 12 hours.

Figure 4. shows a comparison between the average peak amplitude of the detected half harmonic in ex-vivo tissue from 2 s HIFU exposures averaged over either one or two day old tissue which had been degassed for 1 or 2 hrs, respectively. The key aspect of this data is that there does not seem to be a significant difference between the emissions that were detected. There is variation in the uncertainty in the measurements, but this does not seem to be related to the age of the tissue. This analysis demonstrated that the tissue degassing techniques used were sufficient to

enable comparison between acoustic spectra detected from tissue that was either one or two days old.

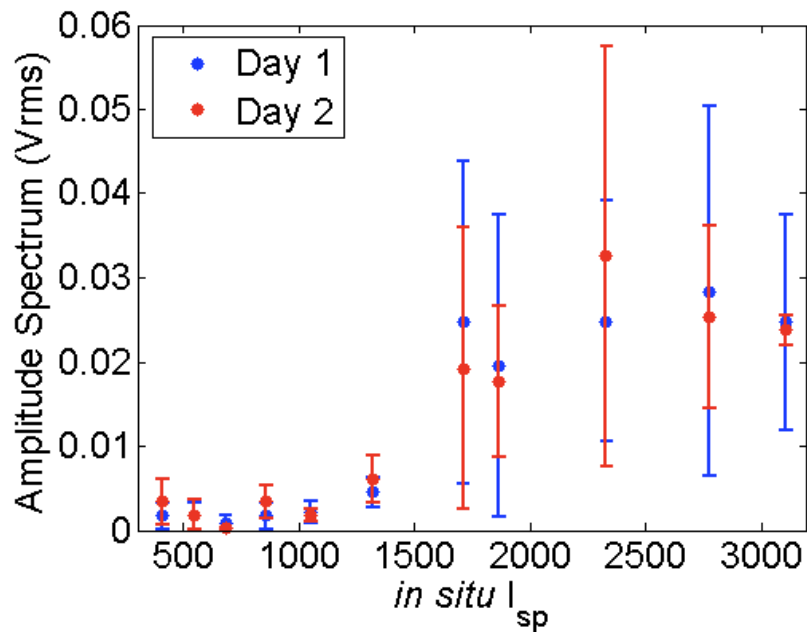


Figure 4. The averaged peak amplitude of the detected half harmonic emissions, separated into exposures performed on 1 and 2 day old tissue. Uncertainty shown in the data is the standard deviation, where the number of exposures ($n = 4-6$).

A specially designed cylindrical Perspex framed tissue holder with acoustically transparent 19 μm thick Mylar windows (front, back, and wrapped around the length of the cylinder – as shown in 5) was used to allow unimpeded HIFU propagation from the front of the tissue sample to its back, while allowing simultaneous diagnostic ultrasound imaging from above. A Perspex tube with a Mylar membrane was inserted into the rear of the holder to hold in place cylindrical tissue samples up to 45 mm in length, but which were compressed to 40 mm in the tissue holder. The tissue was again compressed to 40 mm when the sample was photographed. Each liver sample was subjected to a single 2-5 s long HIFU exposure. Following removal from the holder it was dissected by cutting along the direction of the sound axis to investigate lesion size and shape. The lesion was photographed digitally under polarised light to minimise specular reflections from the tissue surface.

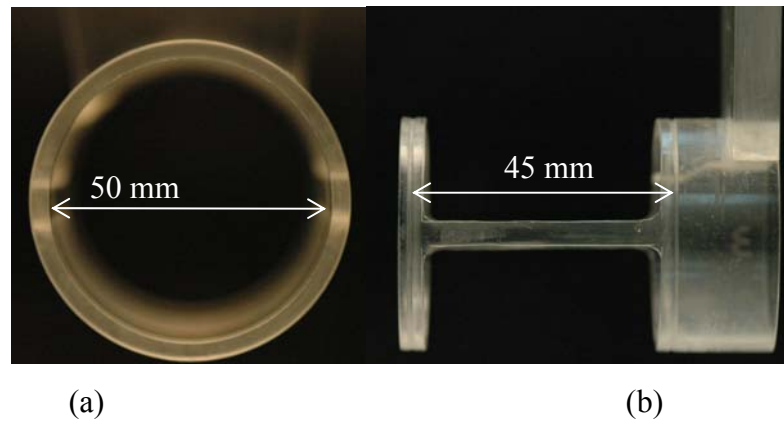


Figure 5. Cylindrical Perspex tissue holder used in both degassed water and ex-vivo experiments. The Front face is shown in (a) and the side view (b) shows length of the holder with the front face to the left hand side and the back face to the right hand side. A diagnostic imaging probe was located above the cylinder at approximately the position of the double headed arrow in (b). For clarity, Mylar windows are not shown in either frame.

In order to obtain independent information about the audible emissions resulting from heating tissue to the boiling point of water, fresh pork was heated in a microwave oven and audible emission measurements were made immediately on its removal. The microphone system described previously was used for this.

A preliminary study found that an exposure time of 120 s at 314 W/cm^2 , resulted in lesion formation in the absence of cavitation. Each tissue sample was exposed once with the HIFU focal plane set 20 mm deep in the tissue. The capsular surface of the liver was always positioned against the face of the holder facing the transducer in order to best approximate the HIFU path through an in-vivo liver. Four second exposures were chosen as these lasted one second longer than the greatest time used previously in a clinical trial (Visioli *et al*, 1999) at the Royal Marsden NHS Foundation Trust. The ex-vivo *in-situ* exposure ranges used were $314\text{-}1000 \pm 50 \text{ W/cm}^2$ (peak negative pressure range 1.52 to 1.86 MPa ± 0.01 MPa), this range being separated into 8 exposure intensities (pressures). Simultaneous and continuous cavitation monitoring during exposure was achieved using: 1 and 10 MHz focused passive detectors, electrical drive power pick-off, audible signal recording (over 1-20 kHz) and a diagnostic ultrasound scanner acting as an active cavitation detector.

2.4 Degassed water studies

Degassed water was exposed to 2 or 4 s HIFU exposures over a spatial peak intensity (I_{sp}) range of 440-2200 ± 50 W/cm² (peak negative pressures of 1.80 to 2.32 ± 0.01 MPa). For a water volume (~ 27000 cm³) significantly larger than the focal volume of the 1.69 MHz transducer (~ 0.3 cm³), it was verified experimentally that repeated exposures in the degassed water did not change its acoustic cavitation threshold over the duration of the experiment. The tissue holder shown in Figure 5 was used for this experiment with the front Mylar window inserted to minimise acoustic streaming. The rear window was not used, in order to allow the ingress of unexposed water and for bubbles to stream out of the holder.

2.5 Sonochemical studies

The 1 and 10 MHz passive sensors with the high and low pass RF filters were used as part of the passive cavitation detection system, as described above. The 1.69 MHz HIFU transducer, and degassed water from the vacuum degassing system described previously were used in these studies. The sonochemical test solution (Potassium Iodide, KI) was mixed to a concentration of 0.1 mmol/dm³ (Birkin *et al*, 2002) in an appropriate volume of pure water (1 L). Individual samples of KI solution (approximately 2 ml) were exposed to 1.69 MHz ultrasound in a specially designed (20x15 mm) holder (Figure 6). The holder was designed such that it enclosed the focal field of the HIFU transducer (16x2 mm) and was sufficiently large that acoustic windows, for monitoring cavitation, could be cut into the sides without loss of its structural integrity, but as small a volume as possible was used in order to maximise the measurement sensitivity. This cylindrical Perspex holder, shown in (Figure 6b) slotted into a Perspex block, which held in place a second piece of Clingfilm covering the rear window. This block was attached to a gantry which allowed positioning to an accuracy of microns, to ensure precise targeting of the HIFU focus within the KI solution.

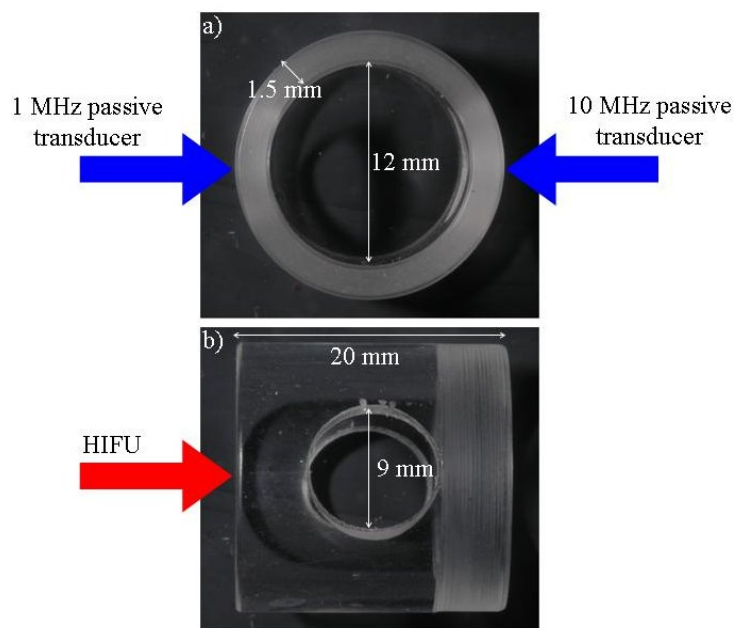


Figure 6. Photographs of the front (a) and side (b) of the cylindrical Perspex holder, which contained the KI solution used for the sonochemical study. The two pieces of cling film used to provide the front sides and rear acoustic windows are not shown in the photograph. The frosted part of the holder shown in (b) was slotted into the Perspex block which held the rear acoustic window in place and located the sample holder in the acoustic field.

The holder was first positioned using the pointer so that the focal peak of the HIFU was located approximately at the centre of the front surface. By using the pulse-echo technique described above to locate the sides of the holder more accurate determination of the centre point of the holder was possible using two opposing pairs of pulse-echo data, typically centre top, bottom, left and right. This was achieved by movement of the micrometer gantry. Once the HIFU beam was aligned with the central axis of the holder it was possible to translate the whole arrangement axially until the focal peak was in the centre of the acoustic windows used for the passive cavitation detectors. Both the HIFU field, and the passive cavitation detectors were aligned prior to the introduction of the KI holder. The sonochemical solution was exposed for 5, 10, 16 or 60 s using an I_{sp} range 440-3100 W/cm² \pm 20% (1.80 to 2.38 MPa \pm 15%) with individual values of 440, 550, 700, 880, 1100, 1400, 1700, 2200, 2500 and 3100 W/cm² (1.80, 1.88, 2.04, 2.08, 2.10, 2.20, 2.30, 2.32, 2.35 and 2.38 MPa). The data acquisition system described above was not able to record continuously for 60 s, so the proprietary software, SBench, was used to acquire ‘snapshots’ of length 4096 points (\sim 0.2 ms) of the acoustic spectra throughout the exposure. 37 datasets were acquired per second at regular intervals, giving a duty

cycle of approximately 1 %. The signal processing techniques described above were used on each of these datasets to obtain the variation with time of the specific peak or bands of frequencies of interest. Once the KI had been exposed to a single HIFU exposure, the 2 ml volume of solution was transferred, using a 5 ml syringe, into a 2 ml Eppendorf tube. The holder was dried thoroughly each time, before being refilled with KI solution for the next exposure.

The relative absorbance between 270-400 nm of the exposed solutions was measured in a spectrometer (UV/VIS Lambda EZ 201, PerkinElmer, Waltham, MA, USA) and was recorded. The quartz cuvette (2 ml volume) used when measuring the spectrum was transparent to the UV spectrum investigated.

3 Results

3.1 Measurements in degassed water

Examples of emissions seen repeatedly during repeated ($n \sim 50$) HIFU exposures of degassed water at three exposures levels are shown in Figure 7 to 11. Figures 12 and 13 show a comparison between the active and passive cavitation detection results for a single exposure. These examples have been chosen as they were typical of the signals detected at these power levels, showing that the amplitude and frequency of the detected emissions increased with intensity.

Figure 7 shows the spectra detected at three different time points during a single 4 s exposure with $I_{sp} = 1100 \text{ W/cm}^2$ (2.10 MPa). Figure 7(a)-(c) and (d)-(f) show the spectra detected using the 1 and 10 MHz transducer, respectively. At 0.3 s, no acoustic emissions were detected above the indicated noise level. Only half harmonic emissions were detected at 0.9 s, whereas 4th, 5th, 6th and 7th harmonics (6.77, 8.47, 10.2 and 11.9 MHz) and broadband emissions (4-12 MHz) were seen at 1.4 s. Figure 8 shows a comparison of the acoustic emissions detected at three different I_{sp} exposure levels (peak negative pressure) at 300 (1.43 MPa), 1100 (2.10 MPa) and 2200 (2.32 MPa) W/cm^2 . This figure shows that as the exposure intensity is increased the amplitude and frequency of incidence of the detected acoustic spectra increase. For the lowest exposure used in this study, (Figure 8a, d and g) no acoustic spectra

above the noise level were detected. Figure 9 shows the expanded electrical drive power measurements for the three exposures shown in Figure 8. In Figure 9(b) and (c), the expanded scales highlight the electrical drive power fluctuations seen. As with the detected acoustic spectra, the increase in the amplitude and frequency of the electrical drive power fluctuations can be seen.

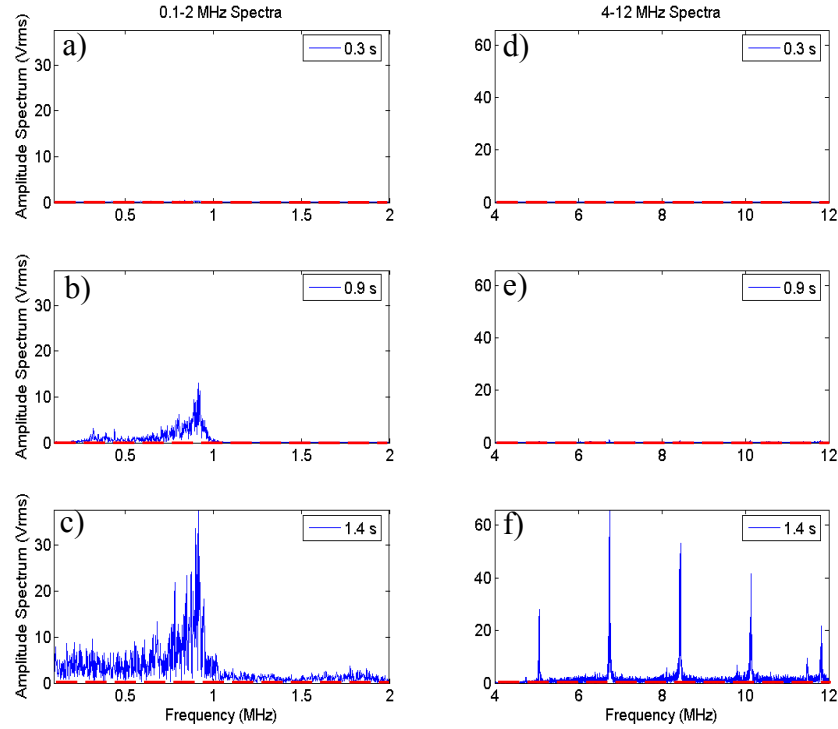


Figure 7. The low (a-c) and high (d-f) frequency spectra detected at three separate times (0.3, 0.9 and 1.4 s) during a 4 s HIFU exposure, [$I_{sp} = 1100 \text{ W/cm}^2$ (2.10 MPa)] of degassed water. A Hanning window function and 2^{13} data points were used to generate each of the FFT spectra. The red dashed line indicates the peak noise level measured during a sham exposure.

The plots show a temporal correlation between the onset of power fluctuations and the first detection of fourth harmonic, broadband emissions and half harmonic emissions at the lower power (Figure 8d-f). The uncertainty in the power measurements was estimated as $\pm 0.2 \text{ W}$, using the highest drive level with a dummy load to mimic the transducer whilst avoiding reflections due to ultrasound exposure. In order to determine whether these power fluctuations coincided with any of the detected emissions it was helpful to expand the time scale as shown in Figure 10.

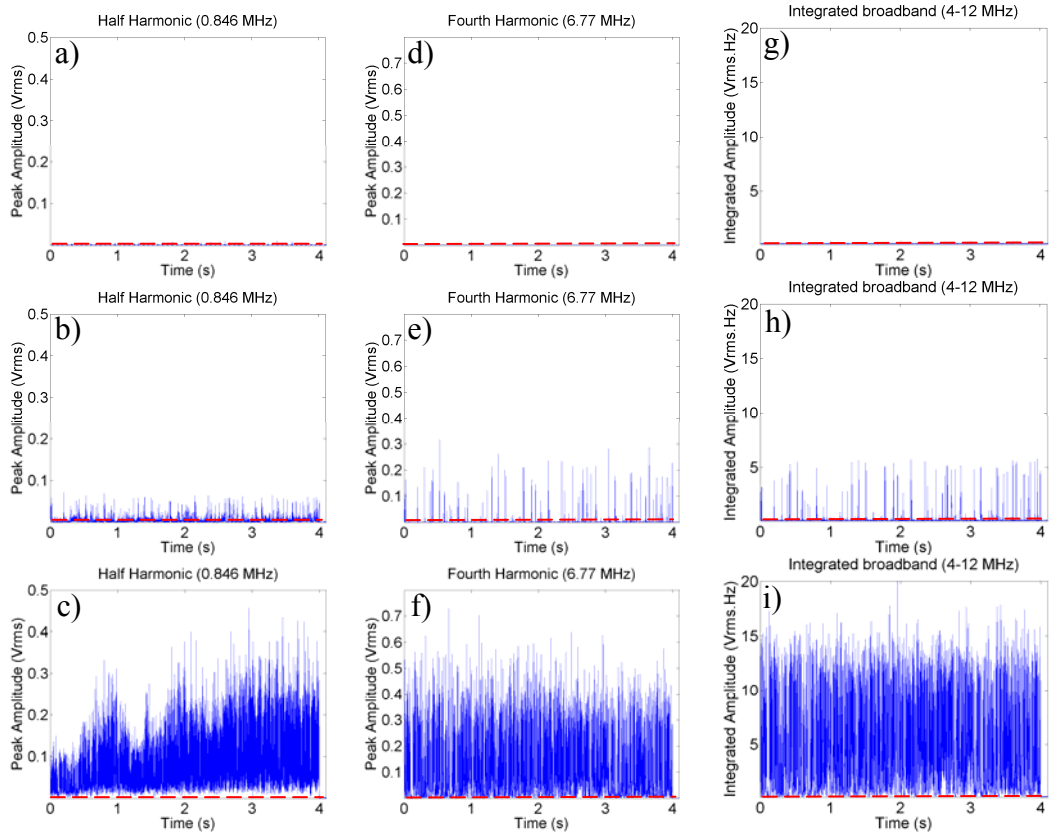


Figure 8. Sample spectra acquired from three individual 4 s HIFU exposures in degassed water, with I_{sp} (pressure) of (a-c) 300 W/cm^2 (1.43 MPa), (d-f) 1100 W/cm^2 (2.10 MPa) and (g-i) 2200 W/cm^2 (2.32 MPa). (a, d and g) Half harmonic (0.846 MHz) emissions, (b, e and h) fourth harmonic and (c, f and i) integrated (4-12 MHz) broadband emissions. The red dashed line indicates the peak noise level measured during a sham exposure.

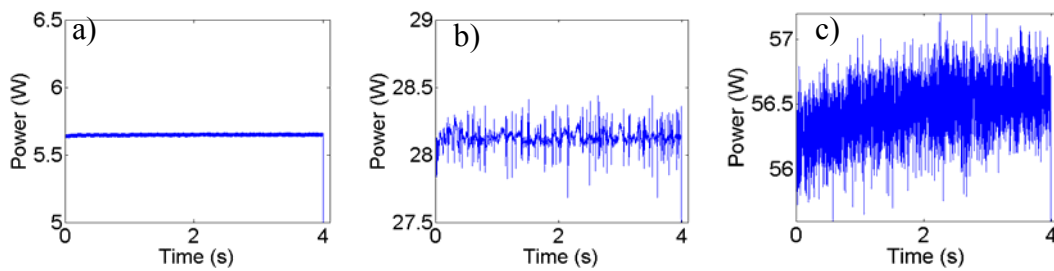


Figure 9. The electrical drive power derived from the measured HIFU drive voltage and current is shown for the three exposures in degassed water shown in Figure 8. (a) 300 W/cm^2 (1.43 MPa), (b) 1100 W/cm^2 (2.10 MPa) and (c) 2200 W/cm^2 (2.32 MPa). The power scale has been expanded to show the range of fluctuation, approximately $\pm 3\%$ about the nominal drive level.

Figure 10 depicts the power fluctuations and acoustic emissions detected between 2.38 – 2.40 s for the 1100 and 2200 W/cm^2 exposures. It shows that the power

fluctuations are initiated at the same time as the broadband and fourth harmonic emissions.

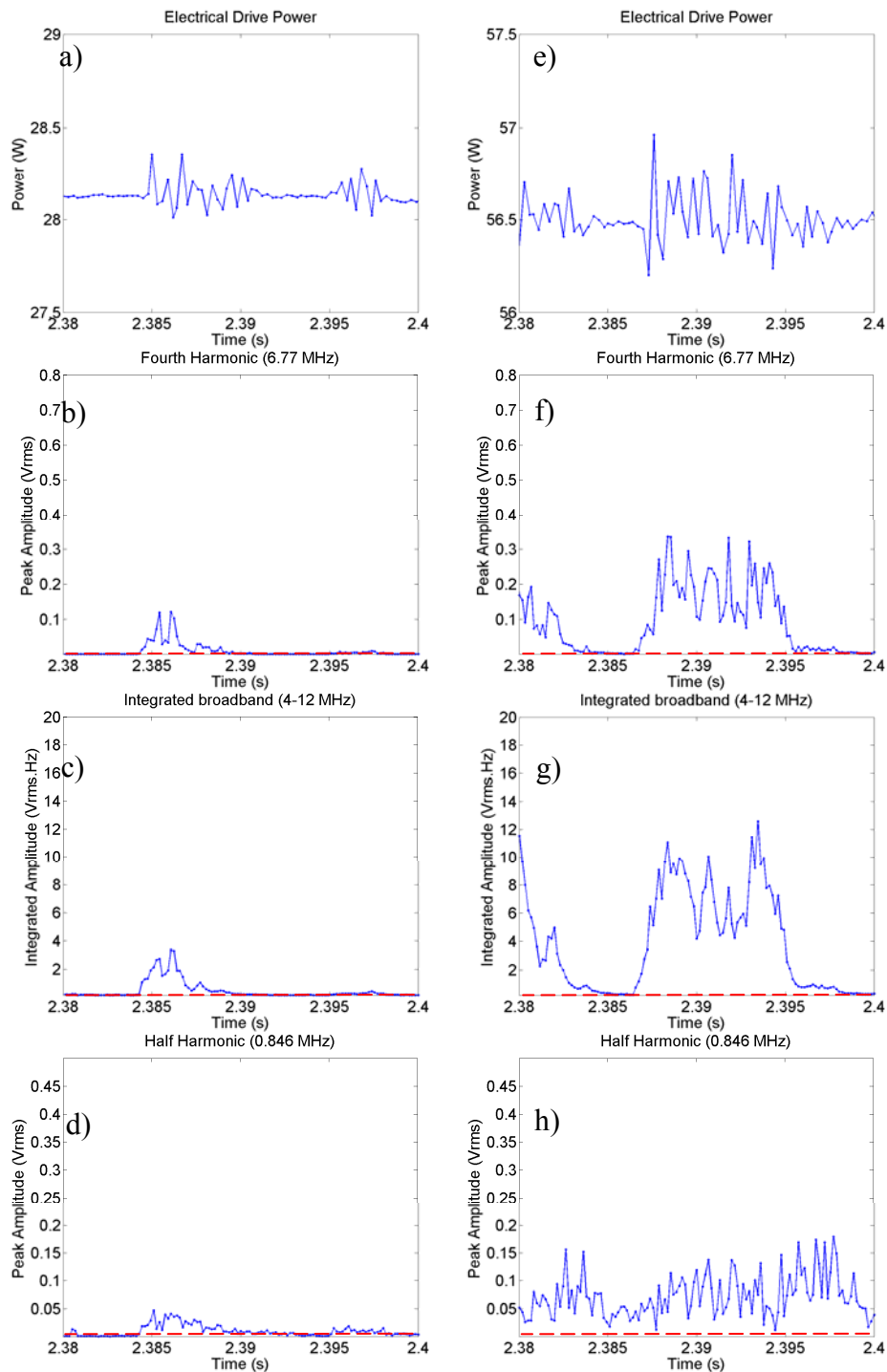


Figure 10. Cavitation monitoring measurements made between 2.38 and 2.40 s into 4 s long 1100 W/cm² (2.10 MPa) (a-d) and 2200 W/cm² (2.34 MPa) (e-h) exposures in degassed water. (a, e) Drive power, (b, f) fourth harmonic, (c, g) broadband emissions and (d, h) half harmonic. The red dashed line indicates the peak noise level measured from a sham exposure.

Figure 11 demonstrates that the majority of the energy in the power fluctuations at both drive levels is at the drive frequency (1.69 MHz).

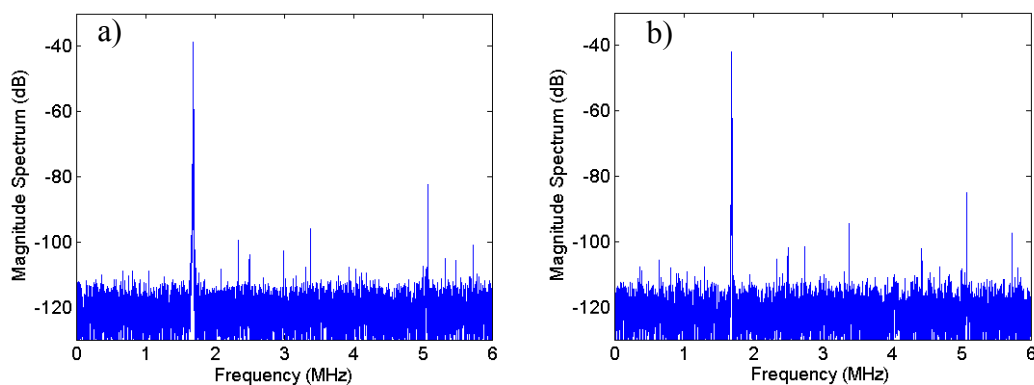


Figure 11. The spectral content of the drive voltage at 2.39 s for (a) 1100 W/cm² and (b) 2200 W/cm² exposures in degassed water. This shows that the fluctuations are dominated by the fundamental frequency (1.69 MHz).

Figure 12 and Figure 13 show a combination of the results of active and passive cavitation detection at two time points (0.21 and 2.43 s) during a 4 s 1700 W/cm² (2.30 MPa) HIFU exposure in degassed water. Figure 12(a) and (c) show the B-mode images acquired at these time points (at a frame rate of 14 Hz, corresponding to a temporal resolution of 72 ms). The interference caused by the HIFU field is present in both images, but its location in the scan is different. Figure 12(b) and (d) show the frequency analysis of these two frames highlighting the frequency band around the second harmonic (3.39 MHz) of the HIFU drive frequency. These images show the location with respect to the HIFU focal peak of the approximate position of the interference. Figure 12(e) demonstrated the audible emissions that were recorded during the HIFU exposure (temporal resolution of 1 ms). Audible emissions are detected intermittently over the 6-18 kHz range, with the peak amplitude frequency at approximately 17 kHz. From the full dataset, where emissions were seen at intervals throughout the exposure, the white boxes highlight the two time points for which the expanded frequency spectra are displayed in Figure 13. The spectra expanded round 0.21 and 2.43 s show that the broadband emissions (4-12 MHz) correlate in time with the electrical drive power fluctuations as seen in Figure 10, whereas the half harmonic emissions (Figure 10b and e) do not. Figure 13(c) and (f) show that the detected broadband emissions are discrete.

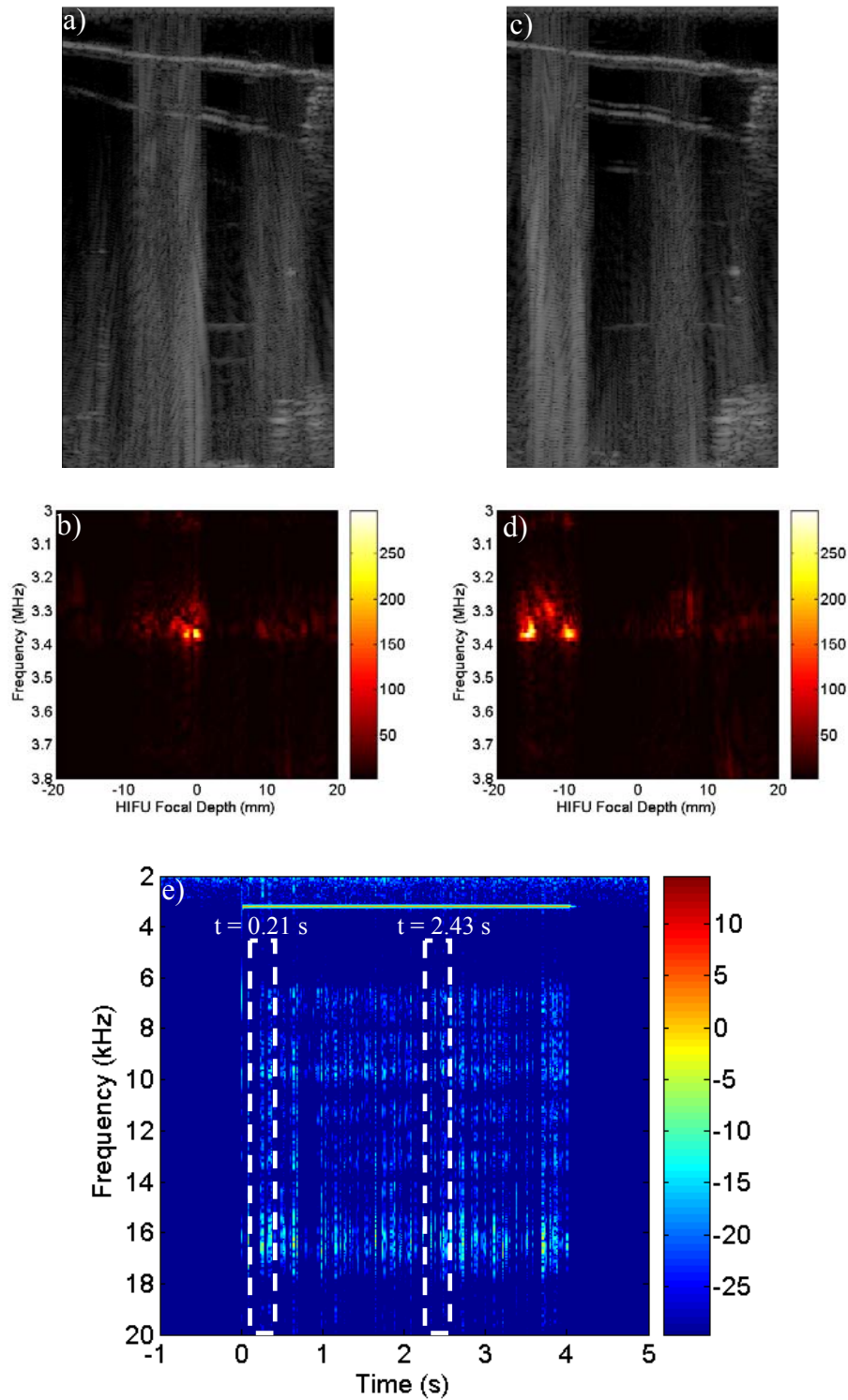


Figure 12. Two ultrasound imaging frames (72 ms resolution) taken during a single 4 s 1700 W/cm² (2.30 MPa) exposure in degassed water 0.21 (a) and 2.43 s (c) into the exposure. Panels (b) and (d) are frequency maps, with a linear colour scale (Vrms), from (a) and (b), respectively. The HIFU focal plane is at 0 mm (in b and d) with the beam incident from the right (in all figures except e). (e) shows the corresponding audible emissions (50 ms resolution), on a power colour scale (dB). The maximum emissions lie between 16-18 kHz.

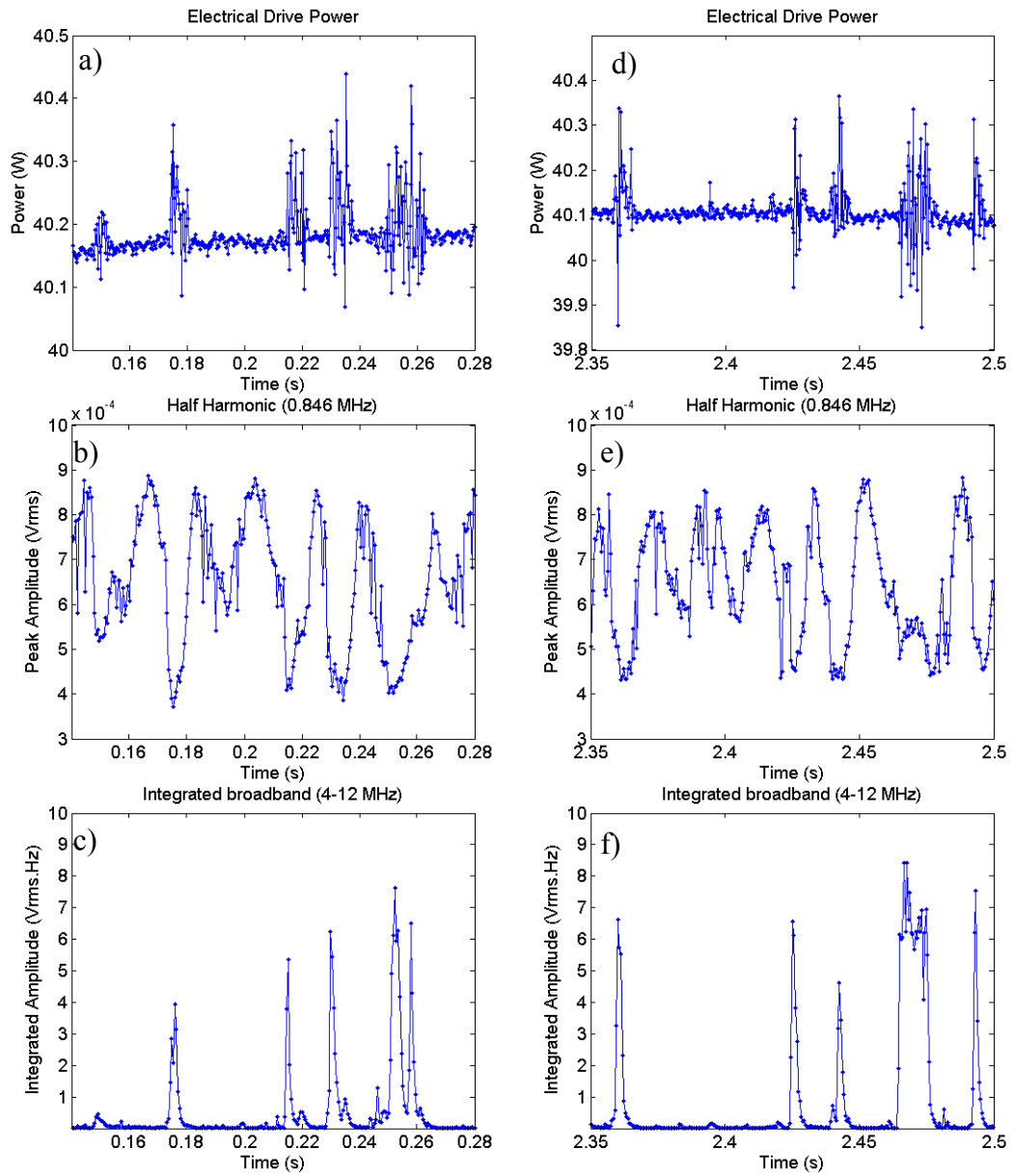


Figure 13. Drive power and acoustic emission data (1 ms resolution) from the exposure shown in Figure 12. The fourth harmonic data has been omitted as it showed a similar trend to the broadband emissions. The time scale was chosen to show emissions at the same times (left column at 0.21 and right column at 2.43 s) as shown in Figure 10, within the temporal resolution of the microphone system (± 0.05 s).

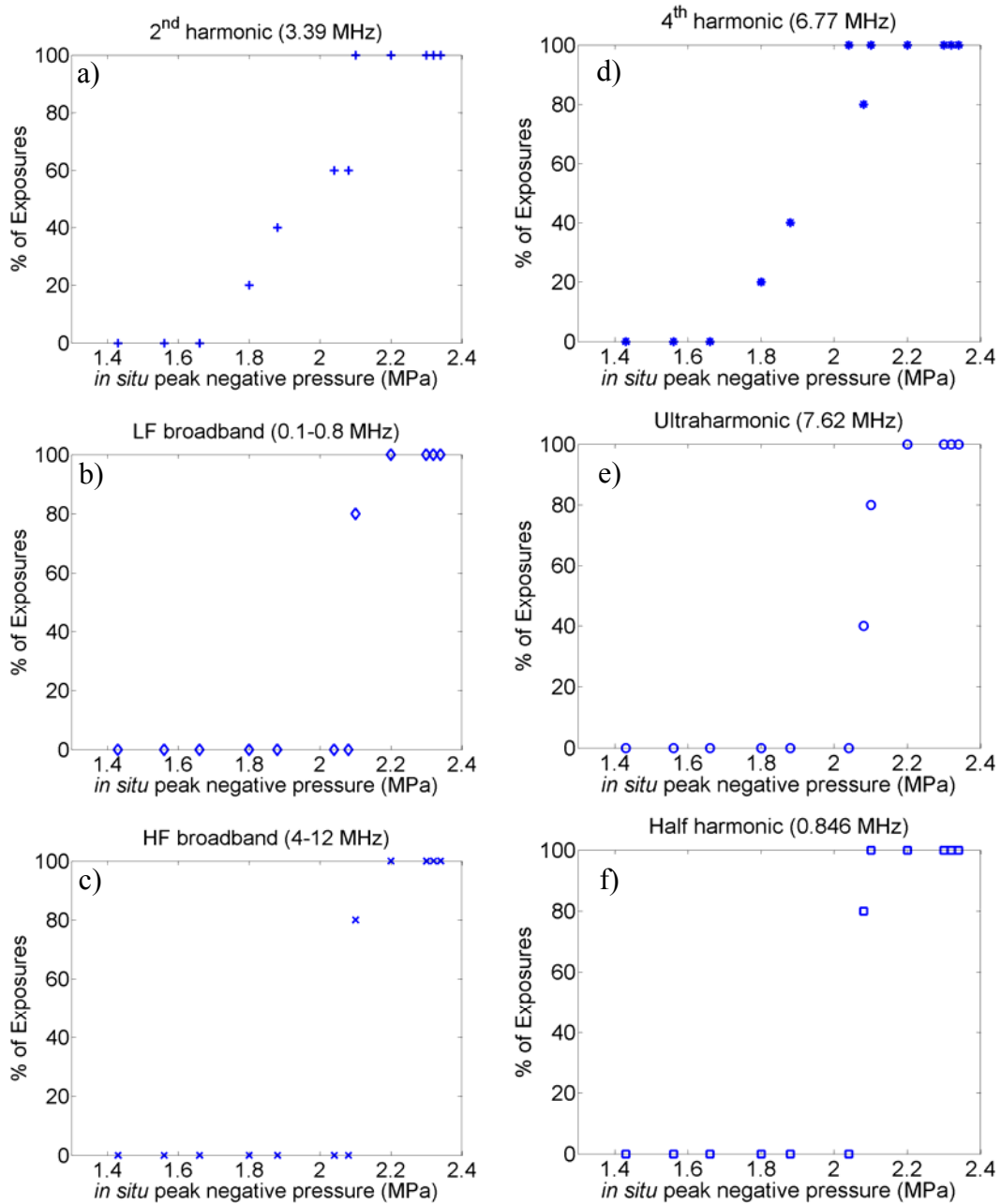


Figure 14. The percentage of exposures in which acoustic spectra with amplitudes exceeding the noise level a minimum of 5 times during the 4 s exposures were detected. The signals were measured over the range 300-2200 W/cm² (1.48-2.32 MPa) where $n = 3-5$ for each exposure level.

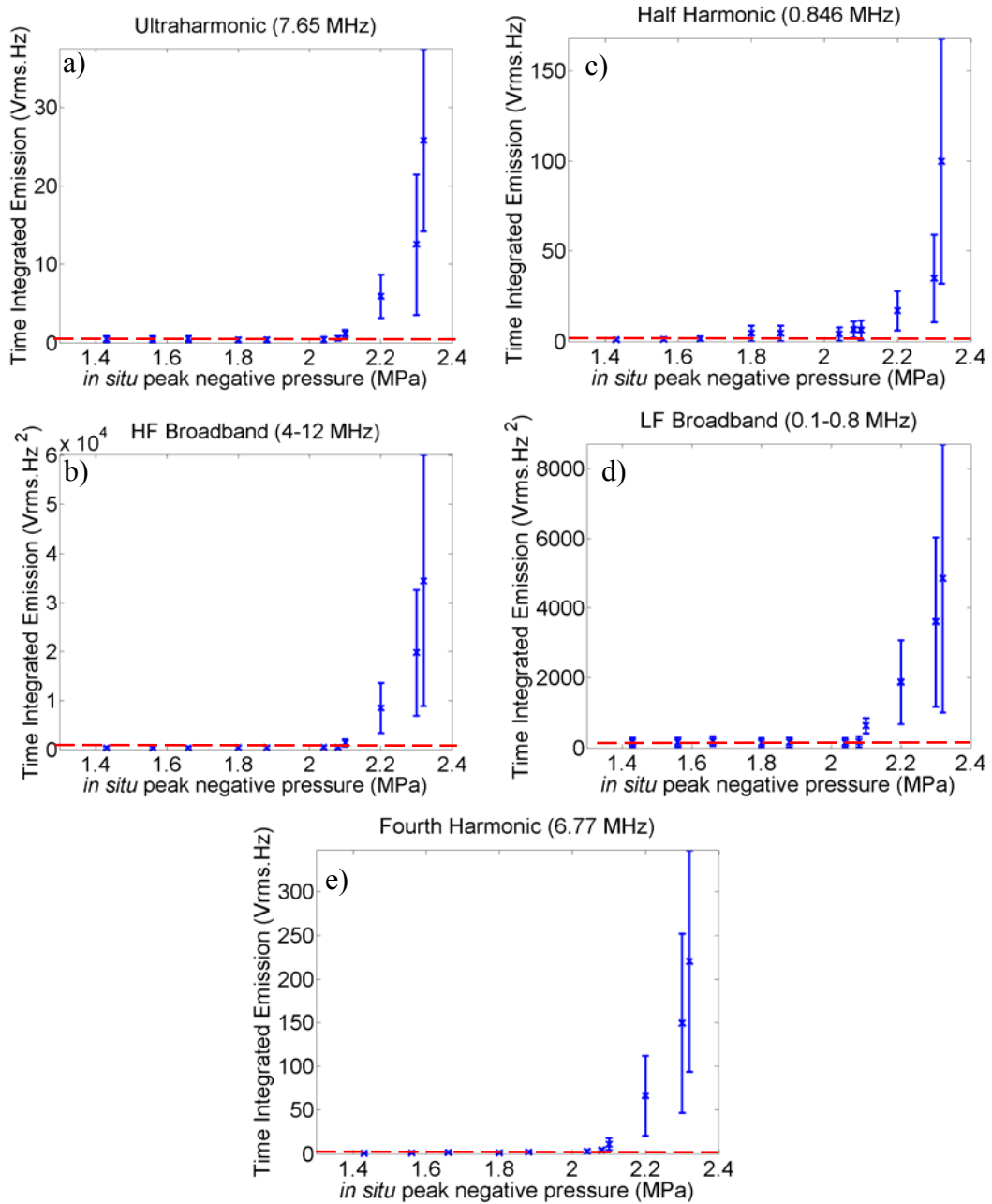


Figure 15. The averaged total time integrated (a) ultraharmonic (7.62 MHz), (b) HF broadband emissions (4-12 MHz), (c) LF broadband emissions (0.1-0.8 MHz), (d) half harmonic (0.846 MHz) and (e) fourth harmonic (6.77 MHz) shown over the range of peak negative pressures used. Uncertainty, where shown, is the standard deviation for $n = 3-5$. The red dashed line indicates the peak noise level measured from sham exposures.

Figure 14 shows the percentage of exposures in degassed water over the exposure range that generated acoustic spectra that were above the detected noise level. The acoustic emissions in these plots show a distinct pressure threshold at which the detected emissions are above the noise level. Once the exposure I_{sp} was equal to or

greater than 1400 W/cm^2 (2.20 MPa), acoustic emissions were detected for 100 % of exposures. Figure 15 shows the averaged emissions integrated over the total time for the acoustic spectra monitored with the dual frequency passive cavitation detection system during all of the 4 s exposures in degassed water. The data show a similar trend to that presented in Figure 14, however the uncertainty in the average measurement increases considerably after 1400 W/cm^2 (2.20 MPa). The red dashed line indicates the peak noise level measured from a number ($n = 3$) of sham exposures acquired throughout the study in degassed water. The average time integrated emissions shown in this figure generally increases with increasing intensity (pressure).

3.2 Sonochemical study

The data presented in this section are from single HIFU exposures, with durations of 5, 10 or 16 s over the I_{sp} (peak negative pressure) range $440\text{-}3100 \text{ W/cm}^2 \pm 20\%$ (1.80 to 2.38 MPa $\pm 15\%$), of a KI solution. Figure 16 and 17 show typical acoustic spectra acquired during two 10 s HIFU exposures of the KI sonochemical solution. These plots are typical in that the peak amplitude fluctuates rapidly during the exposure, in some instances these fluctuations can occur over approximately 1 ms, which is the temporal resolution of this system. In addition, the amplitude and incidence frequency increases with exposure intensity (pressure), as can be seen in the difference between these two plots.

Figure 17(c) shows that the amplitude of the detected half harmonic emissions from this exposure did not drop below the noise level throughout the exposure. The amplitudes of the acoustic spectra shown in Figure 17 were all above the noise level indicated by the dashed red line throughout the exposure.

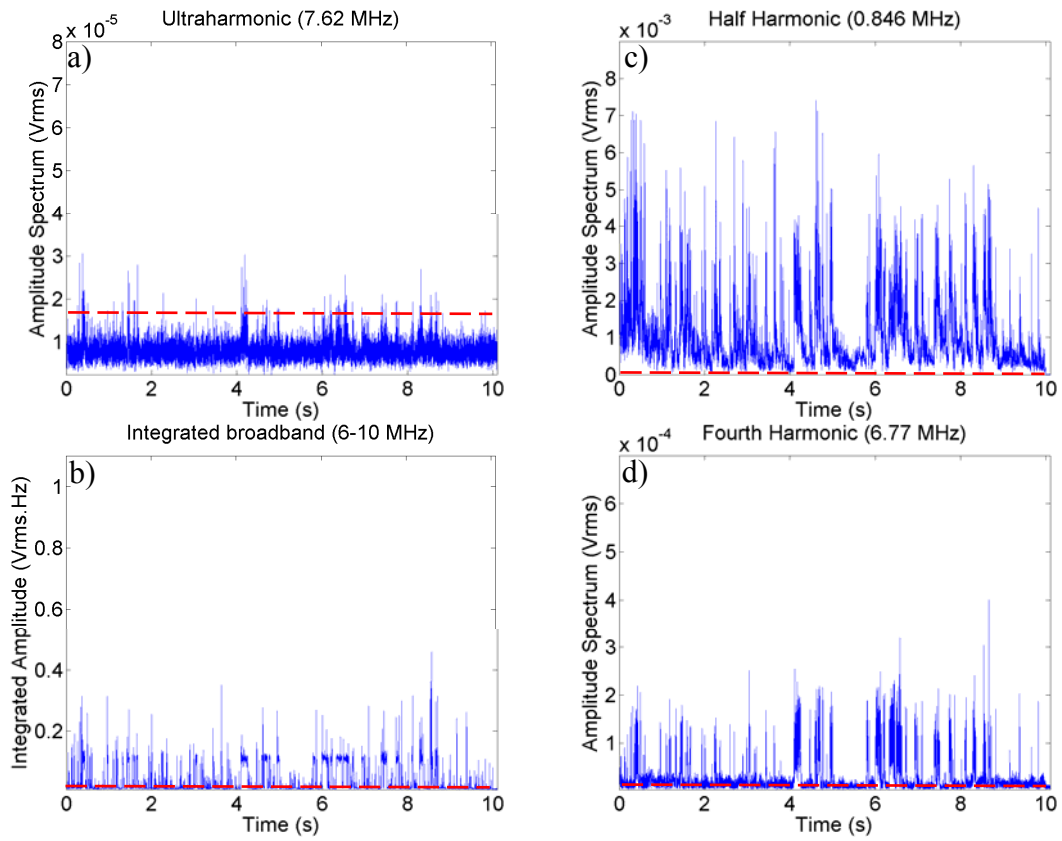


Figure 16. Acoustic spectra detected with the passive cavitation detection system from a single 10 s exposure at 1700 W/cm^2 (2.30 MPa) in the KI solution. The red dashed line indicates the peak noise level measured from a sham exposure.

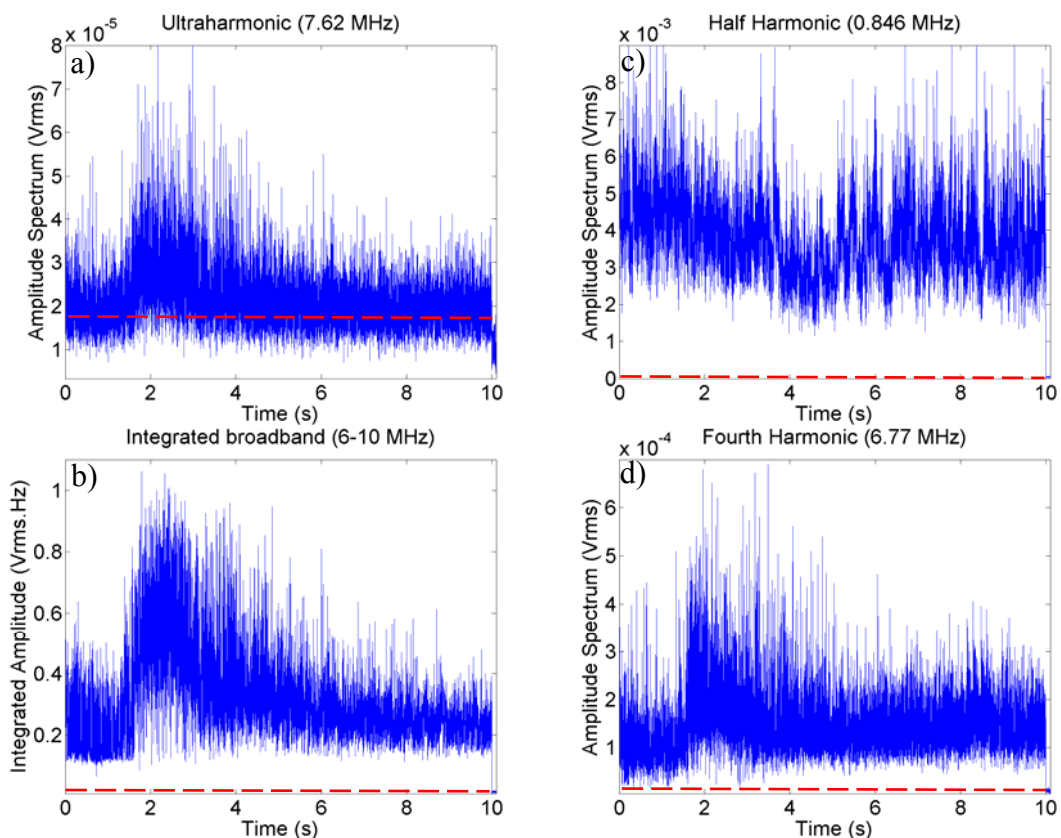


Figure 17. Acoustic spectra detected with the passive cavitation detection system from a single 10 s exposure at 3100 W/cm^2 (2.38 MPa) in the KI solution. The red dashed line indicates the peak noise level measured from a sham exposure.

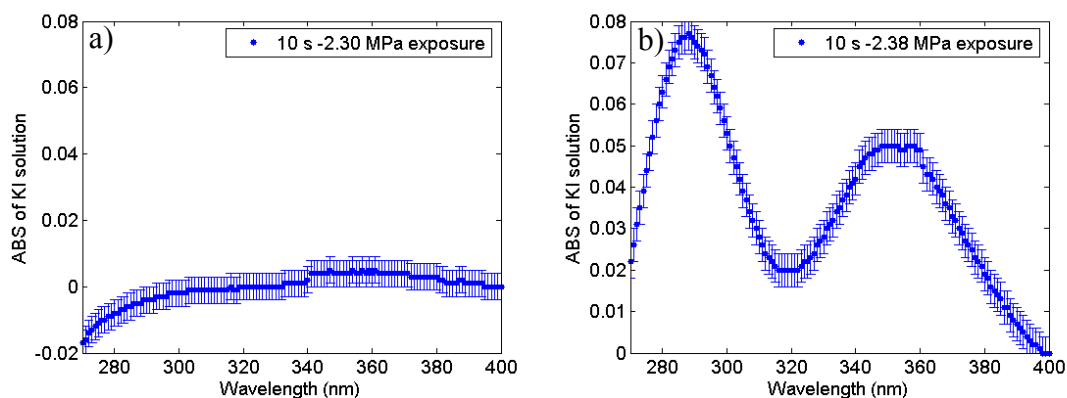


Figure 18. The measured absorbance over the UV spectra of the two KI solutions from the exposures described in (a) **Figure 16** and (b) **Figure 17**. The uncertainty shown in the plots is the measured variation in absorbance at 350 nm of an unexposed sample.

Figure 18 shows the UV absorbance spectra from two KI solutions that were exposed for 10 s to (a) 1700 W/cm^2 (2.30 MPa) and (b) 3100 W/cm^2 (2.38 MPa) HIFU. Figure

18(b) shows the peaks due to the absorbance of light at these wavelengths by the molecular iodine in the solution (Birkin *et al*, 2002), produced by the sonochemical reaction in the solution.

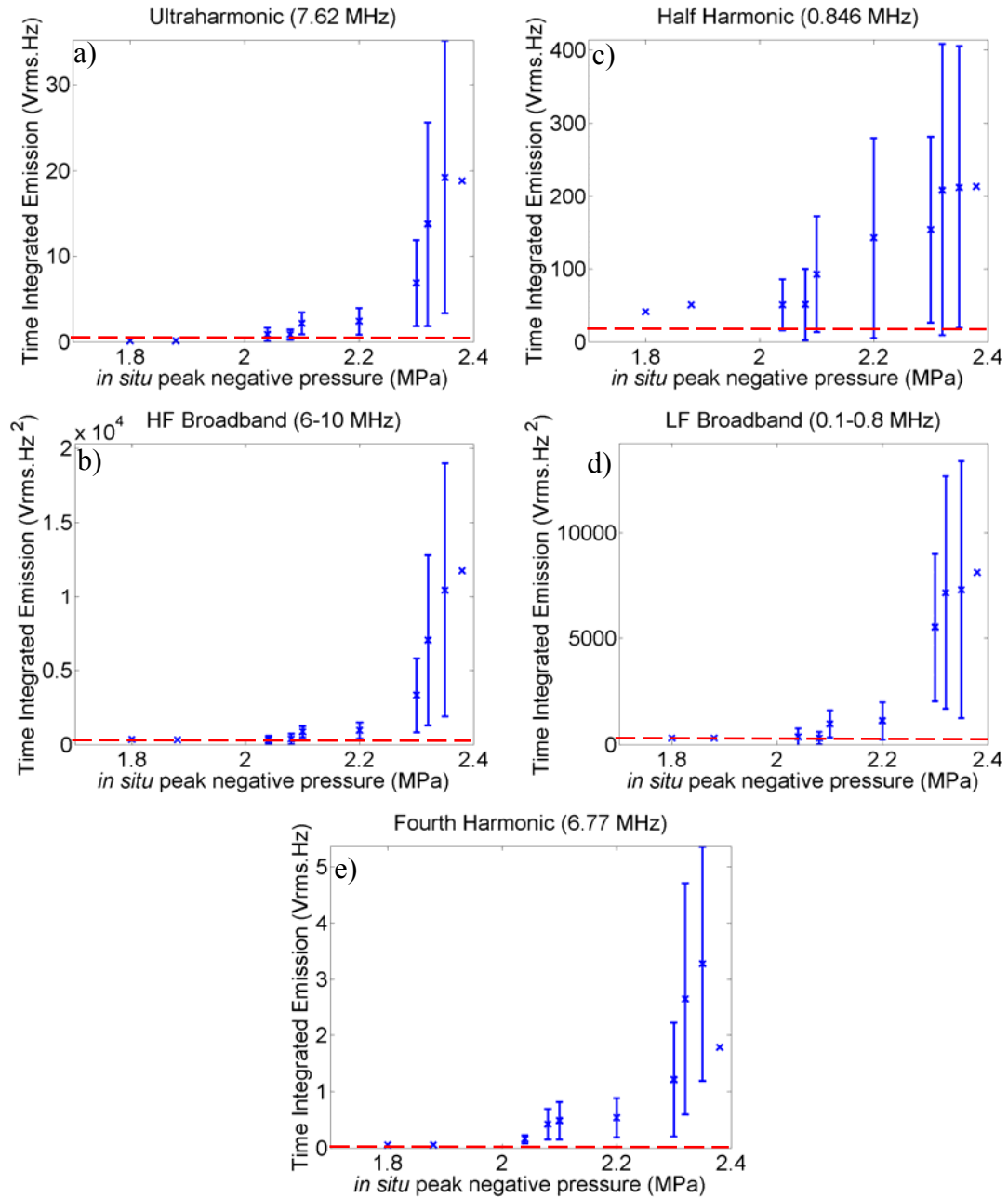


Figure 19. The averaged total time integrated (a) ultraharmonic (7.62 MHz), (b) HF broadband emissions (6-10 MHz), (c) LF broadband emissions (0.1-0.8 MHz), (d) half harmonic (0.846 MHz) and (e) fourth harmonic (6.77 MHz) shown over the range of peak negative pressures used. Uncertainty, where shown, is the standard deviation for $n = 3-5$. The red dashed line indicates the peak noise level measured from sham exposures.

Figure 19 shows the averaged total time integrated emissions for the acoustic spectra monitored with the dual frequency passive cavitation detection system during the 5, 10 and 16 s exposures in the KI sonochemical solution. This shows that half harmonic emissions are detected above the noise level at peak negative pressures greater than 1.80 MPa, while broadband emissions were detected above 2.10 MPa.

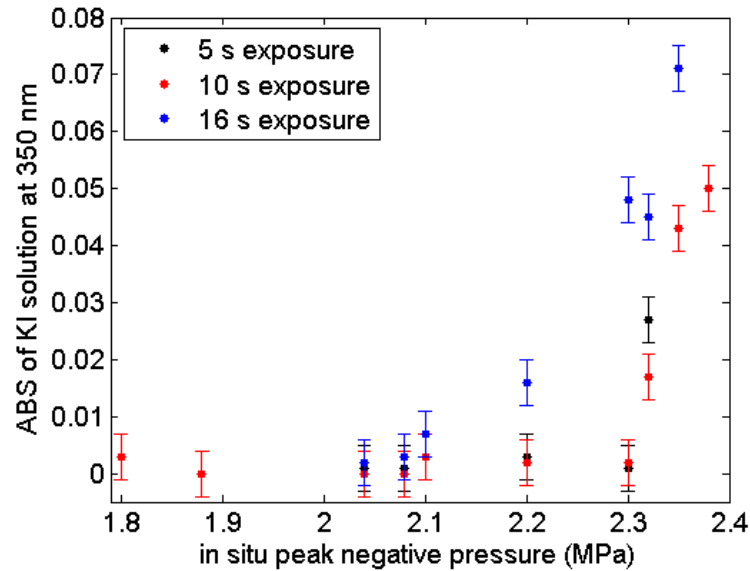


Figure 20. The measured absorbance (ABS) of UV at 350 nm in KI solutions exposed for 5, 10 and 16 s. The uncertainty shown is that of the measured absorbance at 350 nm of an unexposed sample.

Figure 20 shows the measured absorbance of KI samples for 5, 10 and 16 s exposures over the I_{sp} (peak negative pressure) range $440\text{-}3100 \text{ W/cm}^2 \pm 20\%$ (1.80 to 2.38 MPa $\pm 15\%$). For the 5 and 10 s exposures sonochemical change is only seen at 2200 W/cm^2 (2.32 MPa), whereas the 16 s exposures yielded a sonochemical change at 1100 W/cm^2 (2.10 MPa). It can be seen that for the 5 and 10 s exposures where broadband emissions are detected first with the passive cavitation detection system, no change in the absorbance was measured within the uncertainty in the measurements up to 1700 W/cm^2 (2.30 MPa). However, for the 16 s exposures a sonochemical change was detected at the sample pressure level at which broadband emissions are first detected.

3.3 Ex-vivo tissue experiments

The audible emissions detected from microwave heated fresh pork muscle are shown in Figure 21. The signals appear in two frequency bands, the strongest signal being in the 0 to 5 kHz range, with a weaker band from 12 to 16 kHz. Within the strongest signal band, frequencies below 5 kHz are the loudest. When listened to, the emissions were characterised by a ‘hissing’ noise that decreases in amplitude due to the rapid cooling of the tissue, but persists until the end of the recording (recordings of the sound are available at <http://www.isvr.soton.ac.uk/fdag/HIFU.HTM>). This sound is noticeably different from both the audible emissions due to acoustic cavitation activity in water (Figure 12) and is more sustained than the sporadic ‘popping’ noise associated with HIFU boiling in ex-vivo tissue during HIFU exposure (McLaughlan *et al*, 2010).

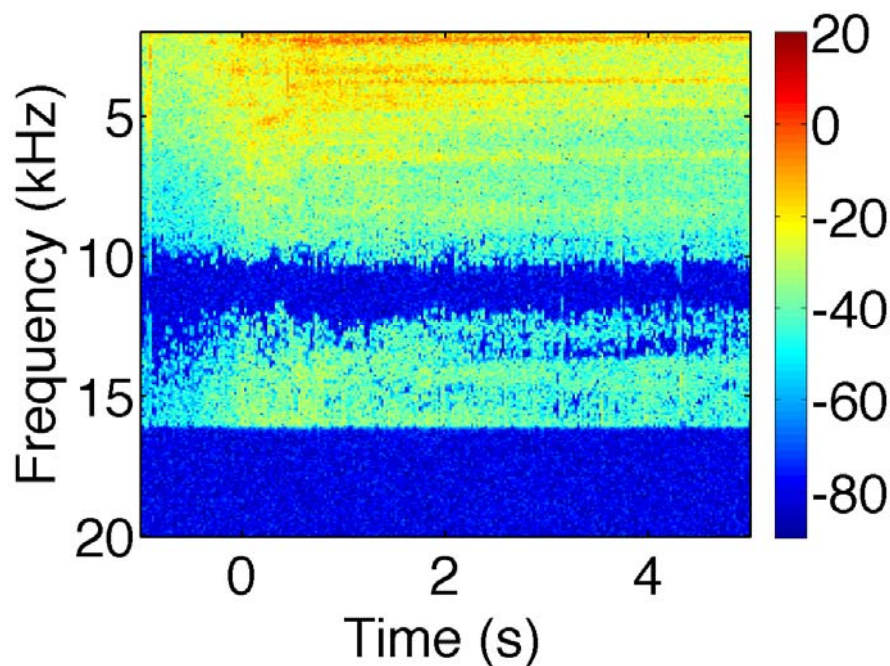


Figure 21. The audible emissions detected (in air) when ex-vivo porcine muscle was heated using microwave energy, shown on a power colour scale (dB) – note that the scale used is different to that for measurements made in water (e.g. Figure 12) and indeed conversion between the two media is not simple (Finfer *et al.*, 2008). Emissions commence at $t = 0$ s when the tissue is removed from the microwave and placed next to the microphone. Signals prior to this time represent background noise in the laboratory.

The results shown here are representative of data obtained from experiments carried out on 20 separate ex-vivo livers, each of which provided 10-15 samples. The ex-

vivo results chosen for presentation here are typical of 3 exposure regimes: 314 W/cm² (1.52 MPa) for 120s, 786 W/cm² (1.77 MPa) for 4s and 1000 W/cm² (1.86 MPa) for 4 s ($n = 3-21$).

For the lowest exposure intensity, 314 W/cm² (1.52 MPa), no half or fourth harmonic, or broadband emissions, monitored intermittently, were detected during the 120 s exposure (Figure 22.) that produced the lesion shown in Figure 6 in McLaughlan *et al.* (2010). For this example it can be seen that the half harmonic emissions are always below the (sham exposure) noise level, and the fourth and broadband emissions do not clearly and consistently exceed the corresponding noise levels.

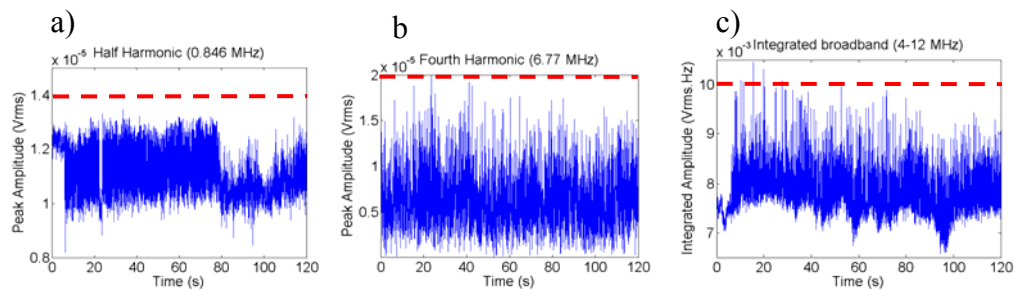


Figure 22. Half harmonic (a), fourth harmonic (b) and broadband emissions (c) for a 120 s free-field exposure at I_{sp} 290 W/cm² (1.32 MPa) in ex-vivo liver tissue. Note the scaling factor of 10^{-5} on (a) and (b). All values plotted on these graphs are either equal to or less than the peak noise level measured from a sham exposure (red dashed line). Diagnostic imaging was not used during this exposure.

There were no detectable audible emissions nor any change in echogenicity between B-mode frames acquired using a Zonare diagnostic scanner (8.5 MHz) immediately before and after the HIFU exposure. The main results of the other ex-vivo studies are presented in the paper by McLaughlan *et al.* (2010), Figures 3 to 7.

4 Theory

4.1 Scattering cross-section

Consider the long wavelength limit ($kR_0 \ll 1$), where k is the wavenumber of the acoustic field (of circular frequency $\omega = 2\pi f_0$) which drives a bubble of equilibrium radius R_0 to pulsate. In this limit the scattering cross-section of a linearly oscillating bubble can be estimated by the following equations (Leighton, 1994):

$$\Omega_b^{scat} = \frac{4\pi R_0^2}{((\omega_0/\omega)^2 - 1)^2 + (2\beta_{tot}/\omega)^2}, \quad (4.1)$$

where the natural frequency for bubble pulsation is

$$\omega_0 = \frac{1}{R_0} \sqrt{\frac{3\kappa p_0}{\rho} \left(1 + \frac{2\sigma}{p_0 R_0}\right) - \frac{2\sigma}{\rho R_0}}, \quad (4.2)$$

In the above formulation and the experiments undertaken here, the medium density is $\rho = 1000 \text{ kg/m}^3$, the hydrostatic liquid pressure is $p_0 = 0.1 \text{ MPa}$, the surface tension is $\sigma = 0.073 \text{ N/m}$, and the polytropic index is κ (which takes a value of $4/3$ for air under adiabatic conditions, and tends to unity under isothermal conditions). The damping is characterised by:

$$\beta_{tot} = \frac{\omega_0^2 d_{tot}}{2\omega}, \quad (4.3)$$

noting that close to resonance the criteria for the use of the $kR_0 \ll 1$ approximation need to be considered very carefully when expressing the scattering through use of such a cross-section (Ainslie and Leighton, 2009). For the experiment considered here, the fundamental frequency of the HIFU field is $f = 1.69 \text{ MHz}$.

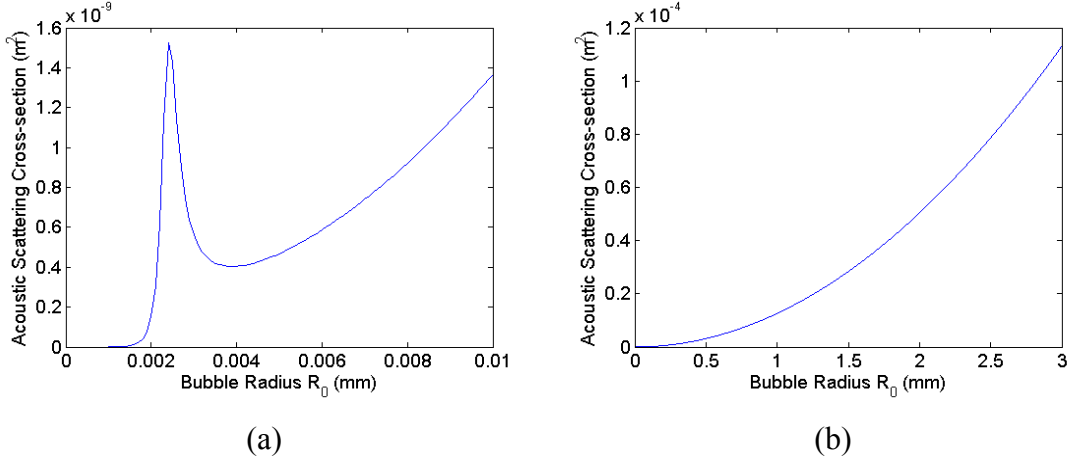


Figure 23. The acoustic scattering cross-sections for a range of bubble sizes, 0.1-10 μm (a) and 0-3.0 mm (b) exposed to 1.69 MHz ultrasound.

Substitution of these values into equations 4.1 to 4.3 allows the acoustic scattering cross-section for a linearly oscillating bubble to be calculated as a function of its equilibrium radius (Figure 23).

The total power scattered (S) from a bubble is given by the product of the intensity in an ultrasound wave (I) (Hill *et al.*, 2004), and the acoustic scattering cross-section (Ω_b^{scat}). For a resonant acoustic cavitation bubble at 1.7 MHz, $R_0 \approx 2 \mu\text{m}$ which (from equation 4.1) gives $\Omega_b^{scat} = 1.5 \cdot 10^{-5} \text{ cm}^2$. For a single bubble generated through ‘boiling’, the equilibrium radius is $\sim 1 \text{ mm}$ (based on the tissue damage observed in Figure 3.8c of McLaughlan *et al.*, 2010), giving $\Omega_b^{scat} = 0.12 \text{ cm}^2$. For an incident intensity of 1000 W/cm^2 on a resonant bubble, the total power scattered and the inverse square law allows estimation of the reflected intensity incident at the HIFU transducer (I_{xdr}). Correcting for the attenuation of a 2 cm liver tissue path, gives an intensity of $I_{xdr} = 15 \cdot 10^{-6} \text{ W/cm}^2$ for a single resonant bubble, whereas for a boiling bubble $I_{xdr} = 0.12 \text{ W/cm}^2$. Thus, I_{xdr} from a single resonant acoustic cavitation bubble is approximately 4 orders of magnitude smaller than that from a boiling bubble.

Assuming that the power fluctuation at 2.3 s, in Figure 3(c) in McLaughlan *et al.* 2010, was caused by a single boiling bubble of radius 1 mm, then it is possible to compare the backscatter caused by boiling and acoustic cavitation bubbles. This event caused peak-peak power fluctuations of 2% of the drive power. The maximum

fluctuation seen in degassed water exposures in Figure 9c (which corresponds with Figure 2o in McLaughlan *et al.*, 2010) was approximately 0.2 %. Making the assumption that these power fluctuations can be compared, it would take an acoustic cavitation bubble cloud with the combined scattering cross-section of $1.2 \times 10^{-2} \text{ cm}^2$ to causes the power fluctuations seen in Figure 9(c) of McLaughlan *et al.* 2010. This would take approximately 800 resonant bubbles.

Power fluctuations have been observed in room temperature degassed water where it is not possible to generate boiling bubbles using HIFU as the heat source. In ex-vivo liver tissue, power fluctuations are only seen when boiling occurs as evidenced by audible emissions and hyperechogenicity in B-mode imaging. In this case I_{xdr} for a 20 mm attenuating liver path from a single resonant bubble is $6 \times 10^{-6} \text{ W/cm}^2$. Despite this $\sim 30\%$ reduction in backscattered intensity (at the transducer) from acoustic cavitation bubbles due to tissue attenuation, it should still be possible to detect power fluctuations in the absence of boiling. Thus, we conclude that backscatter from acoustic cavitation bubbles in tissue does not result in power fluctuations for the exposure conditions used in this paper. This could suggest that there is an insufficiently large bubble population (or coherent bubble behaviour) in attenuating tissue, to give detectable backscatter.

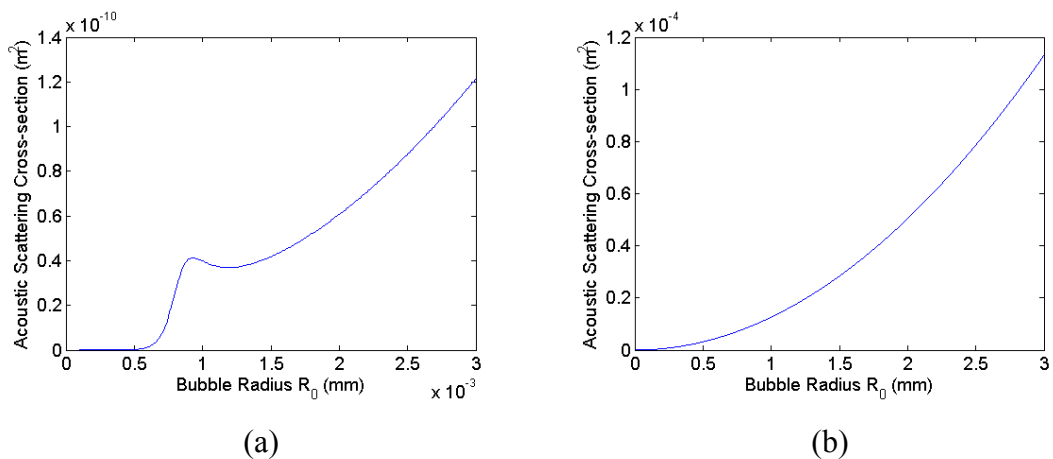


Figure 24. The acoustic scattering cross-sections for a range of bubble sizes, 0.1-3 μm (a) and 0-3.0 mm (b) exposed to 6.77 MHz ultrasound (i.e. the 4th harmonic of the HIFU drive signal).

Using equations 4.1 to 4.3 to calculate the scattering cross-section for bubbles in response to a frequency of 6.77 MHz (4th harmonic of the HIFU drive signal) gives the results shown in Figure 24. These demonstrate that a resonant bubble exposed to an ultrasound frequency of 6.77 MHz has a scattering cross-section which is approximately two orders of magnitude smaller than a resonant bubble at 1.69 MHz (Figure 23a). However there is little difference between the scattering cross-sections of 1-3 mm bubbles at these two ultrasound frequencies (Figure 23b). For this reason, the detected fourth harmonic (Figure 8f) is likely to originate from the non-linear propagation in the HIFU field which is scattered off boiling bubbles.

4.2 Radiated pressure from a resonant bubble

This section further elucidates an argument presented by McLaughlan *et al.* (2010), with clarifying figures which were omitted, for conciseness, from the journal paper. The component of the fourth harmonic arising from nonlinear propagation that is incident on a boiling bubble in the focus of a HIFU beam, can be estimated from hydrophone calibration in degassed water. Using hydrophone calibration data at electrical drive levels equivalent to those shown in Figure 8 (d-f) the harmonic content of the acoustic field could be identified. Figure 25(a) shows the harmonics in the HIFU field in degassed water.

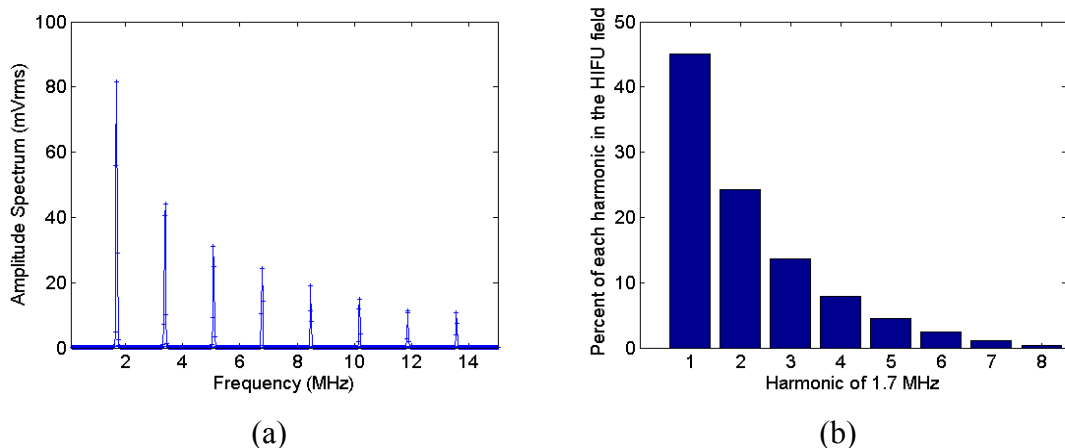


Figure 25. (a) The measured amplitude spectrum (0.01-15 MHz) of individual harmonics, in an 80 cycle HIFU pulse at 47.5 W electrical drive power. (b) Percentage contribution to the time-domain signal of the first 8 harmonics. This was calculated from the total time-domain signal divided by the contribution of each harmonic.

Figure 25(a) shows the V_{rms} voltage of each sinusoidal component of the time-domain signal measured by the hydrophone. Summing the individual harmonic contributions for the first 5 harmonics in Figure 25(b) gives 95% of the total time domain signal. The pressure in the HIFU field was calculated from the measured time-domain voltage signal multiplied by a frequency dependant conversion factor (calibration of the hydrophone provided by National Physical Laboratories, Teddington, UK). This calibration factor fluctuates by approximately 4% over this frequency range (1-9 MHz) and so averaging gives a corrected conversion factor which accounts for 95% of the original time-domain voltage signal. Applying the averaged conversion factor to the time-domain voltage signal gives a total peak positive pressure of 10.5 MPa. From Figure 25(b), it can be seen that the 4th harmonic (6.77 MHz) contributes approximately 8% of the total voltage signal measured by the membrane hydrophone at the HIFU focal peak. Hence, the peak positive pressure component of the 4th harmonic, which could be incident on a boiling bubble (correcting for 2 cm of attenuating medium) is 0.7 MPa. The next step is to estimate the radiated pressure from a resonant bubble at the fourth harmonic (6.77 MHz). Equation 4.4 can be used to calculate the pressure radiated from a bubble (Leighton, 1994).

$$\frac{p}{p_{\infty}} = \frac{\rho}{p_{\infty}} \left[\frac{R}{r} (\ddot{R}R + 2\dot{R}^2) - \frac{\dot{R}^2}{2} \left(\frac{R}{r} \right)^4 \right] + 1, \quad (4.4)$$

where p is the radiated pressure, p_{∞} is the pressure far from the bubble, R is the bubble radius and r is the distance away from the bubble wall. The two terms within the square bracket in equation 4.4, are the acoustic (left term) and the kinetic (right term) components of the radiated pressure.

The Rayleigh-Plesset equation (Leighton, 1994) was solved for a resonant bubble ($R_0 = 0.91 \mu\text{m}$) at 6.77 MHz to give R and \dot{R} . The acceleration term, \ddot{R} was calculated from the derivative of \dot{R} . Figure 26 shows the acoustic and kinetic components of equation 4.4 during a collapse. It demonstrates that the kinetic term of the Rayleigh-Plesset equation is only significant at positions less than a micron from the bubble wall. If we assume that this is an unlikely scenario then any radiated pressure incident

on the surface of a boiling bubble would come from the acoustic term of equation 4.4. Figure 26 shows that the radiated pressure is at a maximum when the bubble radius is near its minimum ($R = 0.25 \cdot R_{max}$). Panel (d) suggests a resonant bubble would need to be less than $\sim 8 \mu\text{m}$ away from the detector in order to produce the same incident pressure on a boiling bubble as the non-linear 4th harmonic of the HIFU field. Alternatively, ~ 100 resonating bubbles, 1 mm away from the boiling bubble would be required to produce the same effect. As discussed in section 4.1, it is likely that the bubble population produced in ex-vivo tissue is insufficient to produce an incident pressure on a boiling bubble comparable to the one generated from the 4th harmonic component of the HIFU field.

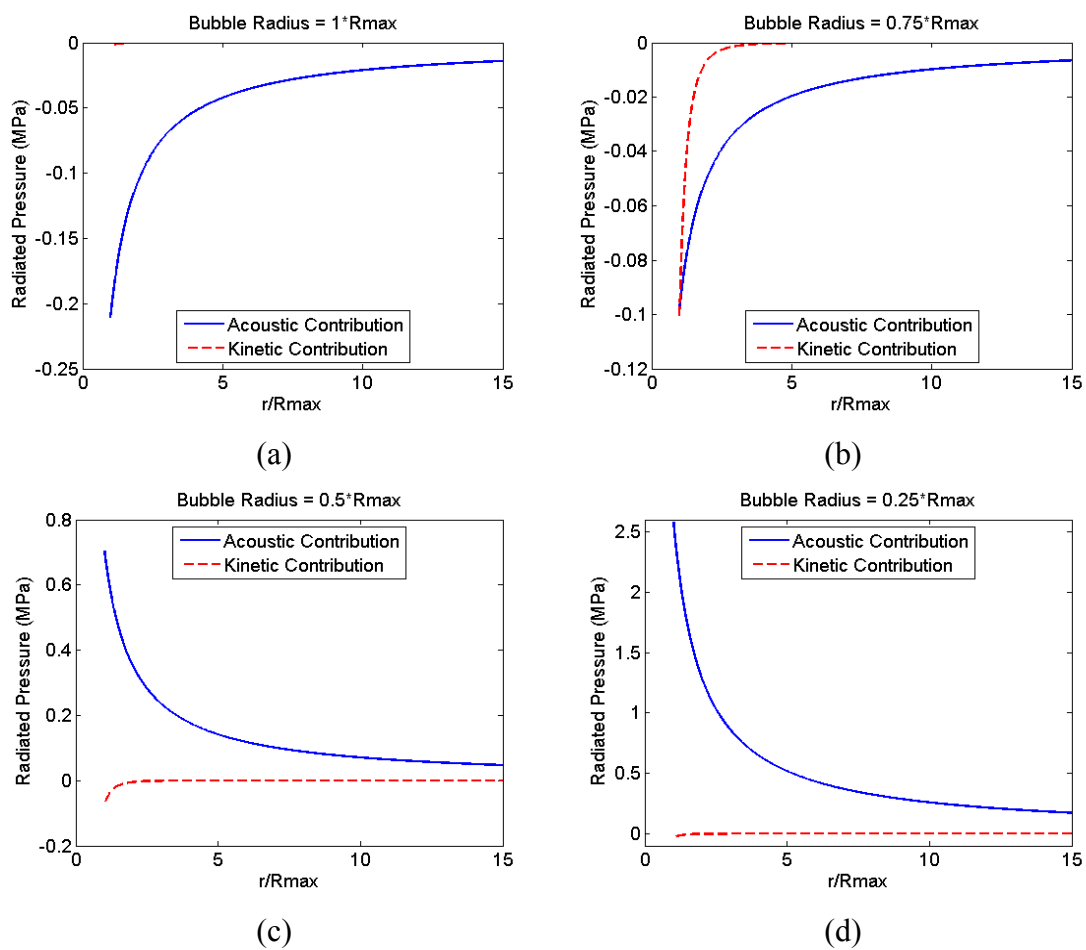


Figure 26. The pressure radiated by a resonant bubble as a function of distance from the bubble wall, r . Four points during the collapse of the bubble are shown, which are $R = R_{max}$ (a), $R = 0.75 \cdot R_{max}$ (b), $R = 0.50 \cdot R_{max}$ and $R = 0.25 \cdot R_{max}$ ($R_{max} = 2.6 \mu\text{m}$).

5 Discussion

5.1 Degassed water studies

The aim of this study was to investigate the relevance of different ways of detecting cavitation activity in ex-vivo tissue, with the eventual goal of determining the best technique for future in-vivo monitoring. Experiments in degassed water are useful for testing a detection system designed for eventual use *in vivo*, since water is a readily available medium and may be used to perform regular quality assurance tests. An advantage of this medium is that it may also be possible to observe cavitation activity directly. The identification of specific cavitation activities was possible using this novel suite of complementary simultaneous cavitation detection methods (acoustic emissions, impedance change, active cavitation detection, and audible emissions). The noise level for the passive detection system was estimated using sham exposures. Twice the measured peak noise value for each signal gave the specified noise floor for this study. Signals detected above this level were designated as detected acoustic emissions only if 5 such events were detected during an exposure duration. This level limits the minimum level of acoustic emission that can be associated with acoustic cavitation. The results of degassed water studies demonstrate how the cavitation detection system behaved in a liquid propagation medium maintained at a constant temperature ($20 \pm 2^\circ\text{C}$). In degassed water, bubbles can migrate more freely than in soft tissue, driven by acoustic radiation forces, acoustic streaming and microstreaming flows, and under the influence of turbulence and buoyancy, the latter being particular potent at removing large bubbles from the acoustic beam. In tissue, such migration is greatly reduced, although temporal changes occur as populations build up, interact with, and disturb, the sound field (see figures 10, 11 and 25 of Leighton, 2007). Once the medium is insonified, fluctuations in the bubble population in water may be expected to occur on a more rapid timescale than in soft tissue, and with less hysteresis (memory). One might therefore expect bubble populations to build up in tissue at a rate not much less than they build up in water, but reduce more rapidly in water once insonification ceases as, for example, buoyancy removes bubbles from the sound field. These processes will contribute to the observed temporal variations in the acoustic emission detected during fixed intensity (pressure) exposures (as shown for water in Figure 7). There is therefore a need for continuous detection of the acoustic

emissions in order to describe the cavitation activity during an exposure as accurately as possible.

Half harmonic (0.864 MHz), fourth harmonic (6.77 MHz) and broadband (4-12 MHz) emissions were detected during a 4 s exposures of $\geq 1100 \text{ W/cm}^2$ (Figure 8). At 300 W/cm^2 (1.80 MPa), no acoustic emissions were detected (Figure 8a, d and g), thus this exposure was deemed to be below the detection threshold for all types of acoustic cavitation activity. Particularly apparent in the 1100 W/cm^2 exposure in Figure 8 is that the detected emissions frequently return to approximately the baseline noise level (dashed red line). This is notably different to the behaviour observed in emissions detected from tissue exposures where the amplitude fluctuates well above the baseline (McLaughlan *et al.* 2010). As discussed above this could be due to the difference in bubble mobility of the two mediums. Doubling the intensity from 1100 to 2200 W/cm^2 result in roughly trebling the magnitude of the detected signals (half, 4th and broadband). A similar trend is seen for the power fluctuations in Figure 9. Figure 10 demonstrates that the drive power fluctuations correlated temporally with broadband emissions and detected 4th harmonic at 2200 W/cm^2 . This leads us to speculate that the drive power fluctuations relate to inertial, but not non-inertial (stable), cavitation. Furthermore, the 4th harmonic and broadband signals appear temporally correlated, suggesting they may occur as a result of the same event(s), whereas the half-harmonic signal does not show the same correlation. We speculate that this correlation probably results from a population of inertial cavitation bubbles acting as scatterers, causing power fluctuations and fourth harmonic signals, in addition to the generation of broadband emissions. Thus, it is likely that this population of bubbles has a scattering cross section of sufficient size to cause a level of backscatter that was detected by the electrical drive power monitoring system. This speculative reasoning is supported by the photographic evidence of Leighton *et al.*, 1989. The two exposures in Figure 10 both show similar effects, however the amplitude of the detected emissions are smaller for the lower exposure. This could be due to a larger cavitating bubble population and/or a more violent collapse from the greater negative pressure. We speculate that the spatial location of events is unlikely to be a dominant factor here. Figure 10 shows that the drive power fluctuations are sensitive to scatter caused by acoustic cavitation in non-attenuating degassed water.

For emissions detected in degassed water, attenuation is negligible. In contrast, emissions generated in liver tissue, either ex-vivo (McLaughlan *et al*, 2010) or in patients, are subject to attenuation that increases with frequency (Hill *et al*, 2004). This highlights a potential limitation for monitoring emissions, such as broadband signals above the HIFU drive frequency, generated from bubble activity deep within tissue (Figure 27). The lower attenuation at the half harmonic suggests that monitoring the broadband spectrum below the HIFU drive frequency may be more effective in patients than monitoring the higher frequency ranges. Alternatively the half harmonic could be used since this indicates the presence of inertial and/or non-inertial cavitation. For the multi-spectrum detection approach described here, testing in water can determine the minimum signals that might be detected in a future clinical system.

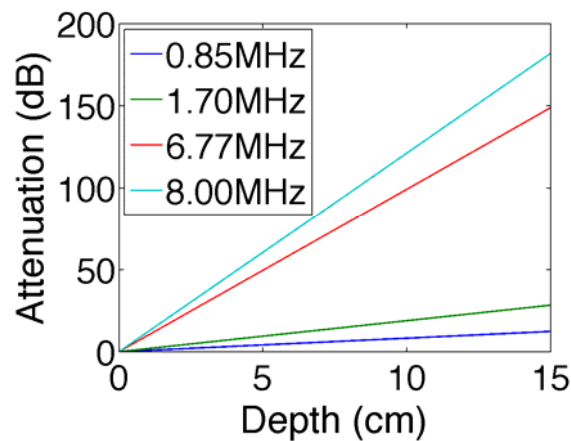


Figure 27. The calculated attenuation at four frequencies with increase depth in liver tissues, which correspond to the half harmonic (0.85 MHz), drive (1.70 MHz), fourth harmonic (6.77 MHz) and the centre frequency of the broadband emission range (8.00 MHz) monitored in this study.

The data in Figure 12 and Figure 13, obtained from simultaneous measurements at 0.21 and 2.43 s, suggest that the increase in the interference pattern of the B-mode images, observed in water, was caused by scattering from acoustic cavitation bubbles (which produced clear broadband emissions at these time points). These plots are representative of results seen at this exposure level ($n = 50$), and show a similar pattern to the higher intensity exposures in Figure 10(e-h). The B-mode frames have a ± 70 ms (14 Hz frame rate) temporal resolution compared to ± 1 ms for the passive

cavitation detection system. Therefore, although it is probable that the events seen in Figure 12(b) and (d) are directly correlated with emissions in Figure 13, it is not certain. Audible emissions (8-20 kHz) were only detected at intensity levels at which inertial cavitation activity was suggested by PCD detection of broadband signals, as shown, for example, in Figure 12(e).

The exposures in Figure 8(d)-(i) both show emissions arising from inertial cavitation activity. The plots, however, show significant differences in magnitude and temporal behaviour. At 1100 W/cm², the detected broadband emissions occur more sporadically than during the 2200 W/cm² exposure. This is most likely to be due to a smaller bubble population and/or less violent collapses. Figure 10 shows the acoustic emissions and power fluctuations for ± 10 ms subsections of data around 2.39 s for the 1100 (a-c) and 2200 W/cm² (d-f) exposures. During this time period, the 1100 W/cm² exposure shows very few acoustic emissions and power fluctuations, even though the exposure is above the inertial cavitation threshold. The 2200 W/cm² expanded plots show that when the amplitude of the broadband emissions are at a minimum, the power fluctuations are also at a minimum. However the half harmonic emissions do not follow the same pattern. This suggests that inertial cavitation plays the dominant role in causing the scatter seen in the power fluctuations and B-mode interference (Figure 12a and c).

Figure 11 shows the spectral content of the drive voltage for the two intensities (1100 and 2200 W/cm²) under consideration. This, and the spectrum of the measured current, showed that only the fundamental drive frequency was detected, potentially as a result of the limited bandwidth of the transducer. This suggests that the power fluctuations were caused predominantly by backscatter of the fundamental frequency, most probably from short-lived bubbles (the source of which is moving stable or inertial cavitation). This preliminary study of the acoustic emissions detected during exposure of degassed water provides an improved understanding of sources of the emissions detected during HIFU exposure. Figures 14 and 15 show the averaged data over all water exposures in two separate ways. Firstly, Figure 14 shows the percentage of repeat exposures that had a minimum of five detected emissions above the noise level. This figure indicates the pressure threshold at which acoustic emissions were

detected. For both the half harmonic and broadband emissions, for different pressure levels, the emissions occurred in a minimum of 80% of exposures giving a very clear distinction between acoustic cavitation occurrence and its absence. Compared with the fourth harmonic, which had a gradual increase in the detected events starting at 20%, rising to 100% in steadily increasing increments. As this signal is dependent on scatter (see section 4) it follows that as the HIFU intensity increases, so does the non-linear components and detection of the fourth harmonic becomes more likely. Figure 15 shows the same data, as an integration of the total detected signal over the exposure time. This approach gives a sense of the total level of cavitation activity, which could possibly be used to identify a therapeutic effect or exposure guidelines. One difficulty lies in the large variability seen in these levels, which is characteristic of stochastic phenomena such as acoustic cavitation.

5.2 Sonochemical study

The sonochemical study provided an independent indicator of inertial cavitation activity with which to compare detected acoustic emissions. Figures 16(b), 17(b) and 18 and show the broadband emissions and absorbance spectra of a sample of KI solution exposed at an I_{sp} of either 1700 or 3100 W/cm² (2.30 or 2.38 MPa) for 10 s. The lower exposure shows no detectable increase in UV absorbance (at 350 nm), despite broadband emissions indicating inertial cavitation. For the higher exposure, there is clear sonochemical activity, and the broadband emissions are higher in amplitude and occur more frequently. At the lower I_{sp} exposure, absence of sonochemical change may be due to the sensitivity of spectrophotometry detection. This is related to the number of Iodine molecules in solution required to cause a change in the absorbance detectable by spectrophotometer. Unfortunately, such data were not available for this device. Another factor to be considered is that the total volume of the solution is approximately 30 times that of the HIFU focal region, and even if inertial cavitation were generated within the focal region, the induced change in the solution might be too dilute for the change to be detected. For an I_{sp} of 3100 W/cm² (2.38 MPa), both broadband emission and sonochemical change were detected. Thus, there is little doubt that acoustic cavitation occurred, and more specifically that it was inertial cavitation.

6 Conclusions

The cavitation detection system described allowed simultaneous active and passive cavitation detection, providing assessment of audible emissions (8-20 kHz), half and fourth harmonic, broadband, drive power fluctuations and B mode image hyperecho (due to both interference from the HIFU beam and changes within the tissue due to bubble formation).

The degassed water studies demonstrated that when inertial cavitation occurred, its characteristic signatures were: audible emissions that were strongest in the 14-18 kHz range, detection of the full spectrum of ultrasonic signals, power fluctuations and localised heightened interference in B mode images. The half harmonic signal showed no temporal correlation with other signals, suggesting that it predominantly originated from stable cavitation events (i.e. those not associated with broadband emissions). The temporal correlation between the other signals suggested that the formation of clouds of inertial cavitation bubbles (emitting broadband signals) resulted in scattering of the drive and its harmonics (notably the 4th harmonic) to the PCD sensors, and the backscatter of the HIFU drive resulting in measurable drive power fluctuations. This was associated with a specific audible emission which could be perceived as a crackle or hiss. Further, but assuming that the activity was mainly along the HIFU focal axis, it was possible to localise the approximate location of the scatterers which resulted in the B-mode interference pattern. The non-linear scatter from bubbles is also supported by theoretical calculations which demonstrated that the non-linear pulsations of bubbles were insufficient to generate the fourth harmonic emission amplitudes, and corresponding drive power fluctuations, seen in this study.

A sonochemical study gave independent verification that inertial cavitation occurred during HIFU exposures in which broadband noise was detected. However, a lack of sensitivity for this optical detection method with the fluid volumes used resulted in a limited ability to validate the detection of acoustic emissions from inertial bubble activity.

The ex-vivo tissue study showed it was possible to create a HIFU lesion in the absence of detectable bubble activity (due to either boiling or acoustic cavitation).

Further it was possible to identify 3 regimes in which very different bubble activities occurred, and these were then used for an in-depth study (McLaughlan et al. 2010).

7 References

- Ainslie, MA and Leighton, TG. Near resonant bubble acoustic cross-section corrections, including examples from oceanography, volcanology, and biomedical ultrasound, *J. Acoust. Soc. Am.* 2009; **126**(5): 2163-2175.
- Birkin, PR, Power, JF, Leighton, TG, Vincotte, AM. Cathodic electrochemical detection of sonochemical radical products. *Anal.Chem.* 2002; **74**(11): 2584-2590.
- Duck, FA. Acoustic properties of tissues at ultrasonic frequencies. In: *Physical Acoustics vol 1, part B* ed. WP Mason, New York: Academic Press, 1990; 73-124.
- Finfer, DC, Leighton TG, White PR. Issues relating to the use of a 61.5 db conversion factor when comparing airborne and underwater anthropogenic noise levels, *Applied Acoustics*, 2008, **69**(5), 464-471.
- Flynn, HG. Physics of Acoustic Cavitation in Liquids. In: *Physical Acoustics* New York: Academic Press; 1964 57-172.
- Hill, CR, Rivens, I, Vaughan, MG, terHaar, GR. Lesion Development in Focused Ultrasound Surgery - A General-Model. *Ultrasound in Medicine and Biology*, 1994; **20**(3): 259-269.
- Hill CR, Bamber JC, and ter Haar GR. Attenuation and Absorption. In: *Physical Principles of Medical Ultrasonics*. Chichester: John Wiley & Sons Ltd, 2004; 93-166.
- Leighton, TG, Walton, AJ, and Field, JE. High-speed photography of transient excitation, *Ultrasonics*, 1989; **27**: 370-373.
- Leighton, TG. *The Acoustic Bubble*. London: Academic Press; 1994.

- Leighton, TG. Bubble population phenomena in acoustic cavitation, *Ultrasonics Sonochemistry*, 1995; **2**: S123-36.
- Leighton, T.G. What is ultrasound?, *Progress in Biophysics and Molecular Biology*, 2007; **93**(1-3): 3-83.
- McLaughlan, J, Rivens I, Leighton TG and ter Haar G. A Study of Bubble Activity Generated in Ex-Vivo Tissue by High Intensity Focused Ultrasound (HIFU). Submitted to *Ultrasound in Medicine and Biology*, (2010).
- Neppiras, EA. Acoustic Cavitation. *Physics Reports-Review Section of Physics Letters*, 1980; **61**(3): 159-251.
- Visioli AG, Rivens I, ter Haar GR, Horwich A, Huddart RA, Moskovic E, Padhani A, and Glees J. Preliminary results of a phase I dose escalation clinical trial using focused ultrasound in the treatment of localised tumours. *European Journal of Ultrasound*, 1999; **9**(1): 11-18.
- Walton AJ and Reynolds GT. Sonoluminescence. *Adv Phys* 1984; **33**: 595-660.